

Global warming: Temperature estimation in annealers

Jack Raymond^{*1}, Sheir Yarkoni¹, and Evgeny Andriyash¹

¹*D-Wave Systems Inc., Burnaby, B.C, Canada*

March 26, 2022

Abstract

Sampling from a Boltzmann distribution is NP-hard and so requires heuristic approaches. Quantum annealing is one promising candidate. The failure of annealing dynamics to equilibrate on practical time scales is a well understood limitation, but does not always prevent a heuristically useful distribution from being generated. In this paper we evaluate several methods for determining a useful operational temperature range for annealers. We show that even where distributions deviate from the Boltzmann distribution due to ergodicity breaking these estimates can be useful. We introduce the concepts of local and global temperatures that are captured by different estimation methods. We argue that for practical application it often makes sense to analyze annealers that are subject to post-processing in order to isolate the macroscopic distribution deviations that are a practical barrier to their application.

1 Introduction

Boltzmann distributions are important in many areas of science, and sampling from these distributions is a major bottleneck in many interesting applications. The tasks of uniform generation, approximate counting, and inference (e.g., estimation of marginal probabilities), are often NP-hard [1, 2, 3]. Heuristic samplers that sample approximately from a Boltzmann distributions are applied in practice to large scale problems (for example in machine learning [4]).

One approach to heuristic sampling is to use an annealer. Whether thermal or quantum, an annealer generates independent samples by slowly transforming an easily prepared initial state into a random final state associated to a given objective function [5, 6]. In the case of simulated thermal annealing (STA), an initial random sample is evolved through a schedule of decreasing temperature towards a specified terminal temperature [6, 7]. In quantum annealing the initial state is a uniform superposition of states, and the final state is a classical sample drawn according to a diagonalized Hamiltonian operator [5]. D-Wave¹ processors are designed to carry out a specific quantum annealing algorithm in a quantum processing unit.

Although annealers have primarily been considered in the context of optimization, they can also be used as heuristic samplers of Boltzmann distributions. Previous studies have indicated that samples produced by the D-Wave quantum annealers may produce samples well described by finite temperature Boltzmann distributions [8, 9, 10, 11, 12, 13].

In this paper we investigate several methods for determining how close sample distributions produced by annealers are to a family of Boltzmann distributions parameterized by inverse temperature β . We evaluate these methods by applying them to the problem of estimating the parameter β best describing samples drawn from an annealer. In particular, we use the latest-model D-Wave quantum annealer the D-Wave 2X (DW2X) [14, 15, 16, 17]. Samples from a classical STA algorithm

^{*}jack.raymond@physics.org

¹D-Wave and D-Wave 2X are trademarks of D-Wave Systems Inc.

are also used to serve as a point of comparison. A simple parameterization for these annealers is studied, sample quality shown here does not reflect performance of suitably-tuned versions of these annealers.

We observe a significant difference between **local** (subspace) and **global** (full space) features of annealer samples when compared to the Boltzmann distribution. We find that even though samples are locally similar to a Boltzmann distribution, the global deviation can be large. Global warming, the fact that global distributional features indicate a higher temperature than local distributional features will be emphasized. For distributions that are close to Boltzmann, we consider several estimators of inverse temperature and evaluate their efficacy. We consider two knobs for each annealer that modify the heuristic distributions generated: rescaling STA terminal temperature, rescaling an analogous DW2X parameter, or changing annealing time (either in STA or DW2X).

By contrasting results from DW2X with STA, we show that differences in annealer dynamics affect temperature estimates in different ways with respect to the two rescaling parameters. However more generally we find qualitative similarities between the two types of annealers on the range and size of problems studied.

We can treat our heuristic samplers as black-boxes and consider temperature estimation as the problem of determining the best fit amongst a single-parameter exponential family of models. This problem has a long history, and best practice is well established [18, 19, 20]. Inference of Ising models parameters under some systematic schemes is NP-hard [21, 18]. However, heuristic approaches such as log-pseudo-likelihood are known to perform well in practice [22], and some schemes are provably convergent with reasonable resources [23, 24]. Bhattacharya et al. [24] recently considered the log-pseudo-likelihood estimator for β and found that estimation based on only a single sample is possible; their focus was primarily on the convergence properties of this estimator. Multi-parameter estimation (estimation of couplings and fields) is more commonly studied, and is pertinent to the class of Ising models we study, though beyond the scope of this paper. In this context, efficient methods of estimation for strongly interacting models include pseudo-likelihood and variational approaches [25, 26, 27].

Many recent papers have shown that physical quantum annealers approximate Boltzmann distributions [8, 9, 10, 11, 12, 13]. In some of these approaches temperature estimators have been developed, and these estimators have been effectively applied in correcting the annealer parameterization, or distribution [8, 11]. A significant focus has been the impact of noise, or systematic specification errors, in the physical annealing implementation [9, 10, 8]. Remedies have been proposed to allow more effective sampling [8, 9, 28], but these methods may not be effective in a scalable manner, or for all problem classes. Some work considering closeness to quantum Boltzmann distributions has appeared [13, 12].

Our paper will be different in that we assume closeness to some classical finite temperature Boltzmann distribution, but use insight specific to annealers in the analysis of deviations and development of temperature estimators. We will show how this approach can yield useful information in the context of both simulated thermal, and physical quantum, annealers. Noise sources and quantum features in physical quantum annealers are important, but will not be the primary focus.

Qualitatively, the deviation of annealing distributions from the Boltzmann distribution for hard-to-sample Hamiltonians has been understood within physics and computer science since the idea of annealers was conceived [6, 5, 7, 13]. As we modify the temperature in STA from its initial value to the terminal value β_T , we move from a distribution where classical states are uniformly distributed to a distribution divided into disjoint subspaces (also called modes, or valleys) of low energy. Under annealing dynamics, a state localized in one subspace cannot easily transition into another subspace that is separated by an energetic barrier once the inverse temperature becomes large (late in the annealing procedure) — this is called *ergodicity breaking* [7]. In the case of STA we gradually decrease the annealing temperature. Temperature is in one-to-one correspondence with expected energy in a Boltzmann distribution, and equilibrated samples are characterized by tight energy ranges. These samples are partitioned into subspaces by the energy barriers as temperature decreases, at which point the samples in each subspace will evolve independently of those in the other subspaces. Rare fluctuations do allow samples to cross barriers, but are exponentially suppressed in the height of the energy barrier later in the anneal. Therefore, the distribution between subspaces will reflect the distribution at the point in the anneal where dynamics between the subspaces became

slow, rather than the equilibrated distribution associated to the terminal model. This effect is called “freeze-out”. We provide a schematic in Figure 1.

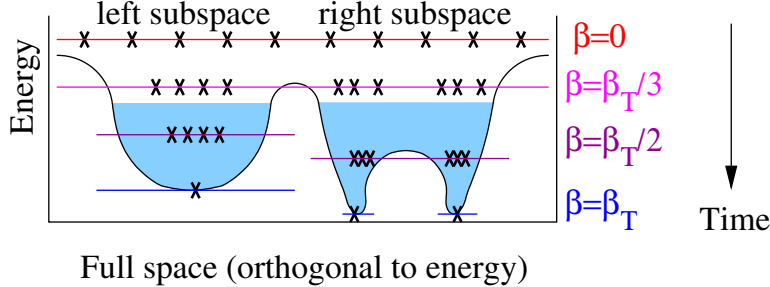


Figure 1: This is a schematic picture to illustrate ergodicity breaking in STA. Proceeding through the anneal, samples evolve according to a schedule from some initial β to the terminal value. In Boltzmann distributions there is an equivalence between mean energy and β [18]. For illustration purposes we take all samples (x) to be concentrated about this mean energy, and show a qualitative distribution over the remainder of the high dimensional space. Initially ($\beta = 0$) samples are uniformly distributed. For small β , samples equilibrate and can explore the entire space on short dynamical time scales. At some later time (in the schematic: $\beta_T/3$) the space may be partitioned into subspaces by energy barriers. At this point, samples can mix rapidly on the left subspace, or the right, but not between. For larger β , in the blue region, dynamics are too slow to allow mixing between the left and right subspaces (ergodicity is broken). The number of samples trapped in each valley is *approximately* controlled by the distribution at the earlier time ($\beta_T/3$) when mixing was still possible. At some later time again ($\beta_T/2$) mixing continues within each subspace. Due to the emergence of a second energy barrier, dynamics become slow on the right subspace (ergodicity is broken again on the right space). Finally, at β_T , the samples are distributed on low energy states, and if β_T is large then all samples converge to their respective local minima. If ergodicity were not broken all samples would converge upon the global minimum. Note that, after ergodicity breaking, each subspace can have a distinct characteristic energy.

Similarly, in the case of quantum annealing, we proceed through a sequence of quantum models of decreasing transverse field (and increasing classical energy scale). From the perspective of the terminal diagonal Hamiltonian, the energy is again decreasing throughout the anneal, and some characteristic mean energy defines the sample set at intermediate stages. Energy barriers become impassable as the transverse field weakens and tunneling becomes slow, so that the process of ergodicity breaking is qualitatively similar. Tunneling dynamics are affected by energy barriers in a different manner to thermal excitation dynamics, which is why there is some enthusiasm for quantum annealing; for some problems it may not suffer the same dynamical slowdown that is true of STA [17].

For many problem classes, these points of ergodicity breaking become well defined in the large system size limit, and can often be directly associated to thermodynamic phase transitions [7, 29].

In this paper detailed consideration is restricted to heuristic sampling from Boltzmann distributions associated to classical Ising spin models. The state x will consist of N spins, defined on $\{-1, +1\}^N$. The Hamiltonian is

$$H(x) = \sum_{ij} x_i J_{ij} x_j + \sum_i h_i x_i, \quad (1)$$

where J and h are unitless model parameters called couplings and fields respectively. The Boltzmann distribution corresponding to this Hamiltonian at inverse temperature β is

$$B_\beta(x) = \frac{1}{Z(\beta)} \exp(-\beta H(x)), \quad (2)$$

where Z is the partition function evaluated at inverse temperature β . Throughout the paper we will use the standard, though improper, abbreviation in which x can denote both the random variable X , and its realization. For experimental purposes we study four paradigmatic Ising models at scales

accessible by DW2X, all with a history in the literature [30, 31, 32, 15], and described in Appendix A.

1.1 Outline

In Section 2 we introduce Kullback-Leibler divergence and mean square error on correlations as measures of closeness to the Boltzmann distribution, and from these develop standard estimators of inverse temperature. Inspired by Benedetti et al. [11], we also introduce a multi-canonical approximation.

In Section 3 we develop self-consistent approximations for efficiently evaluating our inverse temperature estimators; we call these *locally-consistent* inverse temperature estimators. We argue that in the context of annealers the approximation may determine an inverse temperature significantly different (typically larger) than that obtained by a full (computationally intensive) evaluation method. However, we will show that the estimate has meaning in that it captures local distribution features. Applying our approximation to maximum likelihood estimation, we recover in a special case the commonly used pseudo-log-likelihood approximation method.

In Section 3.3 we argue for evaluating post-processed distributions in place of raw distributions, for the purposes of removing superficial differences in the distribution, and for determining the practical (as opposed to superficial) limitations of heuristic annealers.

We then present experimental results relating to our objectives and estimators in Section 4. We conclude in Section 5. Supplementary materials are included in the appendices, and cited at relevant points.

Based on these results we offer the following advice for selecting and interpreting temperature estimation methods in the context of samples drawn from an annealer.

- It is important to define a suitable objective that is minimized by Boltzmann samples, and check that the objective is indeed small for the heuristic sampler for some temperature. Understanding the objective quality of the heuristic sampler will often require input from an independent (exact or heuristic) method. Attempting to quantify error in a self-consistent manner could be misleading.
- Parameters of the heuristic such as the DW2X rescaling parameter, STA terminal temperature, total annealing time, as well as post-processing procedures, should be tuned to the particular sampling objective.
- Temperature can be estimated accurately and efficiently by a local approximation method such as the log-pseudo-likelihood method. If ergodicity breaking is known not to hamper the objective significantly then the local approximation will likely be a sufficient estimate for the entire distribution.
- The multi-canonical method requires additional information and assumptions, and is less established than pseudo-likelihood. However, variations on the pseudo-likelihood method such as these are useful as checks of consistency. Estimator disagreement may reveal ergodicity breaking, allowing us to infer some of its consequences and perhaps adopt remedies.
- Post-processing can move the distribution towards a Boltzmann distribution, locally if not globally. If the heuristic distribution is consistent with some temperature in its macroscopic features, then post-processing at that temperature can correct for local deviations in the distribution.
- A temperature estimator (particularly locally-consistent ones) can be strongly correlated with the temperature used for post-processing. This should be considered when post-processing is invoked.

2 Estimators for temperature

We assume that annealers generate independent and identically distributed samples, according to a distribution P_A . For STA this is reasonable given powerful pseudo-random number generators. For DW2X, correlated noise sources (discussed in Appendix B.2) means this is an approximation that

is more difficult to analyze. In Appendix H we show evidence that these weak correlations in time do not strongly affect our results and conclusions.

We are interested in comparing these heuristic distributions to a family of Boltzmann distributions (2) parameterized by inverse temperature β . Amongst such models we wish to find the best fit, and measure its goodness. We will consider the best temperature to be that which minimizes some objective function. Since the distribution P_A is a heuristic distribution, and not Boltzmann, this temperature may vary between objectives. Given an objective that is minimized at some unique inverse temperature, we then need an estimator for this temperature working on the basis of finite sample sets. An effective estimator should be consistent, with low bias and variance, amongst other criteria [19, 20, 24, 33, 23]. The estimators we study will be consistent, and in some cases optimal with respect to variance and bias (e.g. the Maximum Likelihood estimators [19, 20]). However, characterizing bias and variance will not be a focus of the paper; the main focus of this paper will be on how the inverse temperature is affected by the choice of objective, and how this relates to ergodicity breaking in annealers.

Either to evaluate the objective or to estimate temperature (i.e. minimize the objective) note that we must evaluate some statistics from the Boltzmann distribution, e.g., the mean energy, an energy gap, or marginal distribution. Inference for any of these quantities is NP-hard in the model classes we study. Due to concentration (for larger problems) it is often in practice easier to evaluate the energy, and perhaps $\log(Z)$, than marginal statistics, but estimation of all these quantities is slow in the worst case. For purposes of the models and temperatures explored we are able to accurately estimate the mean energy, $\log(Z)$, or marginal expectations under the Boltzmann distribution by either dynamic programming or parallel tempering [18, 34, 35]. With these values in hand we can efficiently evaluate our temperature estimators, and in most cases the objective (an exception, Kullback-Leibler divergence, is discussed in Appendix F). However, a scalable estimator requires us to find effective approximation methods for these quantities or to define different estimators, and is the subject of Section 3.

2.1 Maximum likelihood (Minimum Kullback-Leibler divergence)

When comparing distributions, a natural objective function to minimize is the Kullback-Leibler divergence (KLD) between the sampled distribution (from the annealer) P_A and the corresponding Boltzmann distribution B_β , as follows:

$$\text{KLD}[P_A, B_\beta] = \sum_x P_A(x) \log \left(\frac{P_A(x)}{B_\beta(x)} \right). \quad (3)$$

The Kullback-Leibler divergence is an important information-theoretic quantity, which places various limitations on the efficacy of P_A for modeling B_β , and vice-versa [18].

P_A has no β dependence, so that at the minimum of this function with respect to β , we obtain an energy matching criterion $\text{EM}(\beta) = 0$, where

$$\text{EM}(\beta) = \sum_x P_A(x) H(x) - \sum_x B_\beta(x) H(x). \quad (4)$$

The energy matching criterion yields the maximum likelihood estimator for β – the likelihood that the annealed samples were drawn from a Boltzmann distribution. Maximum likelihood is perhaps the most well established of procedures for estimating model parameters from data – in this case the data being the samples drawn from P_A [20, 19, 18]. Note that the Boltzmann distribution is an exponential model, and so it is natural to define the estimator in terms of expected energy, which is the sufficient statistic associated to the parameter β [18].

2.2 Minimum mean square error on correlations

In the context of machine learning, an important potential application of annealers, the important feature of samples may be the quality of some statistics that are derived from them. In particular, a machine learning process may require accurate estimation of single variable expectations, and

expectations for products of variables (correlations). For this reason we consider an alternative objective, the mean square error (MSE) on correlations:

$$\text{MSE}[P_A, P_\beta] = \frac{1}{M} \sum_{ij: J_{ij} \neq 0} \left(\sum_x [P_A(x) - P_\beta(x)] x_i x_j \right)^2. \quad (5)$$

We consider specifically the mean error on correlations (excluding errors on single variable expectations) since the models we study experimentally are all zero-field problems so that $E[x_i] = 0$ for all β by symmetry. This objective could easily be generalized to give different importance to different statistical errors. We are presenting an easy-to-understand exemplar. Unlike the KLD, MSE is not a convex function of β in general, although intuitively this might be expected for many problem classes and reasonable heuristics. A derivative of (5) with respect to β will yield a criterion for local optimality. This is a complicated expression dependent on many statistics; in practice, we determine a local minimum by fitting a curve.

We will find that in application to annealers the minimum for this second objective (5) can disagree with the minimum KLD estimator (4), typically being more sensitive to the global distribution features. This is in contrast to the maximum likelihood (minimum KLD) estimators that although sensitive to global features, are also strongly dependent on a local distribution property: whether or not a sample settles towards a local ground state at the end of the anneal.

2.3 Multi-canonical maximum likelihood

Benedetti et al. recently described and applied a method of temperature estimation that exploited samples drawn from two or more annealer distributions, with application to DW2X, where the distributions differed in a rescaling parameter [11]. In the main text we will describe an alternative method, but based on a similar principle, and describe an application and extension of their work in Appendix E.2. These methods are called *multi-canonical* since they involve samples drawn from multiple annealing distributions.

Suppose we are able to draw samples from an annealer at two different parameterizations (A_1 and A_2), each with distributions described by $P_{A_1}(x)$ and $P_{A_2}(x)$. The product distribution can be defined as $P_{A_1, A_2}(x_1, x_2) = P_{A_1}(x_1)P_{A_2}(x_2)$. If both are approximately Boltzmann, this product distribution will be close to $B_{\beta_1, \beta_2}(x_1, x_2) = B_{\beta_1}(x_1)B_{\beta_2}(x_2)$ for some pair β_1 and β_2 . Estimating β_1 and β_2 by maximum likelihood reduces to two independent energy matching criteria. At this stage we have only doubled the work relative to the maximum likelihood estimator. However, suppose we make the assumption that β_2 is some known function of A_1 and A_2 given β_1 . With this assumption we have sufficient information to determine both β_1 and β_2 from a single constraint. Subtracting the conditions for β_1 from β_2 we obtain an energy gap matching criterion $\text{EGM}(\beta_1, \beta_2) = 0$, with

$$\text{EGM}(\beta_1, \beta_2) = \sum_{x_1, x_2} P_{A_1, A_2}(x_1, x_2) [H(x_1) - H(x_2)] - \sum_{x_1, x_2} B_{\beta_1, \beta_2}(x_2, x_1) [H(x_1) - H(x_2)]. \quad (6)$$

The pair of equations $\text{EGM}(\beta_1, \beta_2) = 0$ and $\beta_2 = f(A_1, A_2, \beta_1)$ defines our multi-canonical estimator.

One parameter that can be varied in DW2X is a rescaling parameter r , which is comparable to the STA terminal temperature β_T as discussed in Appendix B.2². Benedetti et al. [11] proposed in their method to use two different values r , and assume that $\beta \propto r$. As is shown later, this assumption does not hold in general even if it were accurate in their application. Note that the criterion (6) is not used in the approach of [11], although both methods require an assumption on the response of β to an annealing parameter.

The multi-canonical estimator has two drawbacks relative to the estimators previously discussed: we require two distributions from the annealer at different annealing parameters and we require an assumption about the response of the annealer temperature to changes in the annealing parameters.

²In practice our DW2X rescaling parameter r is a rescaling of the Hamiltonian submitted to DW2X.

3 Local approximations for evaluating objectives and estimators

The problem with the objectives and estimators outlined in Section 2 is that their use requires inference with respect to the Boltzmann distribution that is independent of the heuristic annealer, and that is NP-hard to perform.

In this section we show how, beginning from the annealed distribution, we can build a reasonable approximation to the Boltzmann distribution and thereby evaluate the estimator self-consistently. The estimators are motivated as approximations to those of Section 2. However, the approximation can be weak and may lead to a predictable deviation in the estimate.

3.1 Single distribution statistics by self-consistency

Our estimators and objectives require us to evaluate statistics of the annealed distribution P_A . Estimates of mean energy or correlation based on P_A can be obtained by evaluating those statistics from the sample set $\mathcal{S} = \{x\}$, or equivalently, evaluating their corresponding expressions using the plug-in estimator to P_A :

$$\hat{P}_A(x) = \frac{1}{|\mathcal{S}|} \sum_{x' \in \mathcal{S}} \delta_{x,x'} . \quad (7)$$

The quality of estimates depends on variance and sample size. Since we use sample sets of size 10^4 we find this not to be a significant barrier to temperature estimation and evaluation of the objectives in our experiments. One exception is the KLD objective, which requires us to estimate an entropy $-\sum_x P_A(x) \log P_A(x)$. In Appendix F we discuss why evaluation is problematic with a plug-in estimator (7) and propose a mitigation strategy.

We must also evaluate energy, correlations and $\log(Z)$ under the Boltzmann distribution, which is NP-hard. However, under the assumption that $P_A(x)$ is close to the Boltzmann distribution we may make a *locally-consistent* approximation. The local approximation to $B_\beta(x)$ is

$$\hat{B}_\beta(x) \propto \sum_{x'} \hat{P}_A(x') W_\beta(x|x') , \quad (8)$$

where W_β is a β -dependent kernel. It efficiently maps any state into a new state, with the property that the distribution is unchanged if it is a Boltzmann distribution

$$B_\beta(x) \propto \sum_{x'} B_\beta(x') W_\beta(x|x') . \quad (9)$$

The transition kernels used in Markov chain Monte Carlo (MCMC) methods are suitable candidates for W_β [7, 29]. The blocked Gibbs MCMC method is described in Appendix B.1. The simplest example of W_β is conditional resampling of a single variable, which is an element in the blocked Gibbs sampling procedure. All variables except i are unchanged, and i is resampled according to the conditional Boltzmann distribution $B_\beta(x_i|x \setminus x_i)$ given the neighboring values:

$$W_\beta(x|x') = B_\beta(x_i|x'(\neq x_i)) \prod_{j(\neq i)} \delta_{x_j,x'_j} . \quad (10)$$

Applying the approximation (8) in combination with the kernel (10) to maximum likelihood estimation, and taking an average of $\text{EM}(\beta)$ for each possible variable i , we recover the maximum log-pseudo-likelihood (MLPL) estimator [22, 24]. The MLPL estimator is normally derived and motivated slightly differently. We discuss this in Appendix C, and present a concise form of (4) under this approximation.

For our purposes, the MLPL estimator is a special case of a more general *locally consistent* estimator. We choose a kernel, approximate B_β (8), and then evaluate the energy matching criterion (4). The locally consistent approach can also be applied straightforwardly to the MSE, and minimum MSE estimator, of Section 2.2. We will, however, restrict attention to the MLPL estimator throughout our experimental studies, except in Appendix D, where we consider the effect of a hierarchy of increasingly powerful kernels.

Consider the following interpretation for the role of the kernel: We take every sample that the annealer produces, and conditionally resample according to W_β . We then take this new set of samples as an approximation to Boltzmann samples drawn according to B_β . Since W_β obeys detailed balance, it necessarily brings the distribution towards the Boltzmann distribution, but for practical W_β not the whole way. Consider again Figure 1, and note that resampling single spins, or doing some other efficient conditional resampling procedure (i.e. some short-run MCMC procedure) does not lead to a significant macroscopic redistribution of the samples, except in the high-temperature regime where fast dynamical exploration of the space is possible. Thus, the approximation (8) will typically inherit the macroscopic bias of the sampling distribution through \hat{P}_A . However, through the kernel there is a local redistribution of the samples. The locally consistent estimator is therefore effective in capturing any *local* deviation in the distribution P_A not representative of B_β .

3.2 Multi-canonical statistics by self-consistency

In the case of the multi-canonical estimator of Section 2.3 we again must infer a mean energy difference between two Boltzmann distributions to evaluate the energy gap matching criterion, which is NP-hard. A kernel can again come to our rescue. This time we are inspired by the kernels from multi-canonical MCMC, such as parallel tempering [34, 7]; other choices that depend on the terminal temperatures (as opposed to simply the gap in the terminal temperatures) could also be considered. In effect we employ the following identity for Boltzmann samplers:

$$B_{\beta_1, \beta_2}(x_1, x_2) \propto B_{\beta_1, \beta_2}(x_2, x_1) \exp((\beta_1 - \beta_2)[H(x_1) - H(x_2)]). \quad (11)$$

We complete the approximation by replacing B_{β_1, β_2} in (6) by the identity (11), with a plug-in estimate for \hat{P}_{A_1, A_2} (7)

$$\begin{aligned} \text{EGM}(\beta_1, \beta_2) = & \sum_{x_1, x_2} P_{A_1, A_2}(x_1, x_2)[H(x_1) - H(x_2)] - \\ & \frac{\sum_{x_1, x_2} P_{A_1, A_2}(x_2, x_1) \exp\{(\beta_1 - \beta_2)[H(x_1) - H(x_2)]\} [H(x_1) - H(x_2)]}{\sum_{x_1, x_2} P_{A_1, A_2}(x_2, x_1) \exp((\beta_1 - \beta_2)[H(x_1) - H(x_2)])}. \end{aligned} \quad (12)$$

The energy matching criterion can now be solved for $\Delta\beta = \beta_1 - \beta_2$, and will have a finite solution provided the energy distributions of the two annealing parameterizations overlap significantly. We expect an intermediate amount of overlap in the distributions is ideal to extract the maximum signal just as it is ideal for implementation of multi-canonical MCMC methods [34, 7]. Various works have considered how to extract maximal information from multi-canonical distributions, this might also inform a better choice of kernel [33, 11].

If we know β_1 for annealer condition A_1 (or β_2 for annealer condition A_2) then we can find the complementary inverse temperature. As a simple example, suppose for A_1 we set the DW2X rescaling parameter $r = 0$ (or $\beta_T = 0$ for STA), we would reasonably expect to recover $\beta = 0$, thereby the gap would be precisely β_2 . Alternatively, we can make an assumption on the estimate β as a function of the annealing parameters, in order to extract one of the two end values.

This method gives a mixture of some global and some local information, but the features of the distribution it may capture are rather difficult to interpret in general. Appendix E discusses this further, alongside experimental results and a discussion of the method of Benedetti et al. [11].

3.3 Towards global distribution features

Objective functions such as maximum likelihood and minimum mean square error on marginals are influenced by a combination of local and global distribution features. We have already seen that locally consistent estimators can assign a meaningful temperature for local deviations from the Boltzmann distribution, but may fail to capture macroscopic features. It would be useful to have an objective, or estimator for temperature, that reflects only the macroscopic distribution features. One way to do this is to manipulate P_A so that the local distributional features are removed.

We have also not considered so far the practical application of annealers other than in the choice of objective. By our definition, for an annealer to be useful it must have a good objective value,

and also be fast in generating samples. However, these two aims are typically in tension. A method that allows one to trade off these two goals is post-processing. In post-processing we take individual samples, or the set of all samples, and apply some additional procedures to generate an improved set of samples. This requires additional resources and can be heuristic, or employed in a manner guaranteed to improve the objective.

Those distribution features that can be manipulated by post-processing will be called local distortions. Local, since it is assumed the post-processing will not be so powerful as to manipulate the macroscopic distribution. One generic and potentially detrimental distortion in annealers is local relaxation: the tendency of states to decrease in energy towards their local minima at the end of the anneal as illustrated in Figure 1.

Post-processing has two uses considered here: to extract macroscopic distribution features (by discounting local distortions), and to improve the heuristic distributions. As shown in Appendix F it can even be used to reduce bias and variance on estimators. A post-processed distribution can be represented as

$$P_{\beta,A}(x) = \sum_{x'} W_{\beta}(x|x') P_A(x') , \quad (13)$$

where W_{β} is again a kernel.

Note that in development of the locally-consistent estimator (8) we employed a kernel W_{β} as a trick to approximate B_{β} . In post-processing we are interested in the ability of W_{β} to generate a new distribution that is assumed to be distinct from the Boltzmann distribution and to which we wish to assign an objective value and temperature.

Implicit in our definition (13) is a restriction to “do no harm” post-processing. If we are seeking to compare the distribution against a Boltzmann distribution B_{β} , then the post-processing is considered to do no harm if it meets the criterion (9). In the case that W_{β} involves only conditional resampling according to B_{β} (rule (10) is one such case) it is straightforward to show that the $\text{KLD}[P_{\beta,A}, B_{\beta}] \leq \text{KLD}[P_A, B_{\beta}]$, that the distribution is improved in KLD. It is reasonable to expect, though not guaranteed, that other objectives will improve under do no harm kernels. Heuristic approaches without such guarantees may sometimes do better in practice, but carry risks.

For purposes of isolating macroscopic features of the distribution it is ideal to apply enough post-processing to remove the local distortions; but leave the macroscopic features intact. This is a balancing act that strictly exists only as a concept, since the distinction between local and global is blurred except perhaps in the large system size limit. We will show in experiments that weak post-processing known to not significantly impact the macroscopic distribution does dramatically change the local distribution, thereby having an impact on the likelihood and MSE objectives and associated estimators.

For purposes of improving the heuristic, W_{β} should be chosen powerful enough that the time-per-sample is not significantly impacted. One sweep of blocked Gibbs sampling, though not necessarily the most powerful, meets the criterion of being a small overhead in time per-sample for DW2X and STA under the operation conditions we examine.

With a self-consistent definition of β we must take into consideration the dependence of $P_{\beta,A}$ on β in objective minimization, and so the energy matching conditions (4) and (6) are modified. For the case of KLD minimization, the new energy matching criterion, and a simplified form for the KLD, are discussed in Appendix F.

In Section 3 we developed self consistent estimators. We emphasize that with post-processing, these estimators become to a large extent redundant, unless the post-processing method kernel (13) is significantly weaker than the kernel used in the self-consistency trick (8). Since post-processing redistributes the samples locally according to β , and our approximators (under the self-consistent approximation) are sensitive only to this local effect, we should expect the local estimator to return a value very close to β regardless of the macroscopic features, and any initial local distortion of P_A . The discussion has focused on single distributions in this section, though it would also be straightforward to consider multi-canonical post-processing as well.

4 Experimental results

In this main section we consider only two models, RAN1 and AC3, which are spin-glass models compatible with the DW2X topology (explained fully in Appendix A). We consider DW2X with its annealing schedule chosen for optimization purposes, as described in Appendix B.2. At points we also consider this schedule slightly modified, either by changing the rescaling parameter or by modifying anneal duration. We consider standard STA procedures parameterized at least in part with reference to DW2X, an optimization context as well as runtime considerations were involved in the choice of parameters, as described in Appendix B.1.

Either of these two annealers might be significantly improved for sampling or inference applications by modifying easily accessible annealing parameters. It is not the aim of this paper to discover these optimal settings; rather, we use simple default settings that make phenomena easier to identify, interpret and reproduce. Problem classes have also been chosen with this objective. We therefore strongly advise the reader against drawing conclusions about the effectiveness of STA versus DW2X as samplers, based on the untuned (and untimed) versions here, and the restricted set of problem classes and post-processing investigated.

4.1 Maximum likelihood and maximum log-pseudo-likelihood estimation

The maximum log-pseudo-likelihood (MLPL) estimate is efficient to evaluate, and here we compare it to the more computationally intensive maximum likelihood (ML) estimate. This section shows that the two methods indicate best fits to significantly different β . We consider variation of the DW2X rescaling parameter r and the STA terminal temperature β_T for our annealing procedures on 100 randomly generated RAN1 problems at each of 3 sizes: C2 (32 variables), C4 (127 variables), and C12 (1100 variables). RAN1 is a spin-glass problem commonly studied for D-Wave processors described in Appendix A. Results for a different spin-glass model, AC3, are shown in Appendix G.

We can first consider the behavior of thermal annealers with a range of terminal inverse temperatures. Nominally they sample from the terminal model, but with larger terminal energy scales (larger r or β_T) we expect them to fall out of equilibrium and be characterized by an intermediate value of β due to ergodicity breaking. Figure 2 shows the ML and MLPL estimates based upon the same sample sets. We see that the MLPL estimates follow a linear curve, which would indicate that the terminal model is indeed the best fit to the samples. By contrast the ML estimator indicates values that have a concave relation with the target model. The maximum likelihood estimate is smaller, presumably reflecting the range of inverse temperature for which dynamics slowed down. This is consistent with the fact that the non-linearity is less pronounced for smaller systems.

The ML estimates by contrast indicate that by increasing the terminal inverse temperature we cannot decrease temperature beyond some limit. The mean energy improves little, owing to states being dynamically trapped near local minima of high energy. The MLPL estimate provides a misleading picture that by increasing β_T we emulate Boltzmann distributions of larger β more effectively. The MLPL estimator does not distinguish a local minimum from a global minimum, and so returns a higher estimate.

DW2X can also be manipulated by setting the rescaling parameter r on the interval $[0, 1]$. We thus repeat this experiment using sample sets from DW2X. In Figure 3 we see that both locally (MLPL) and globally (ML) the estimators are concave as a function of this rescaling. Like the STA case, estimates are consistently larger for MLPL than ML, and decrease for larger more complicated problems, but only modestly so in the case of MLPL. A naive interpretation of the rescaling parameter might lead to a general hypothesis that $\beta \propto r$, where the constant of proportionality can be determined by the terminal energy scale in annealing. As discussed in Appendix B.2 this should not be expected in general, and these results are explained by the *single qubit freeze-out* as discussed in Section 4.2. In Appendix G we show the result for the AC3 problem class, and find a trend much closer to linear, which can again be explained in the context of single qubit freeze-out.

The difference between the MLPL and ML estimates is further explained qualitatively in the schematic Figure 1: We believe the phenomenon to be similar in both DW2X and STA, although the interaction of the dynamics with the energy landscape may be quite different. When ergodicity is broken, and the sample set is divided over subspaces, each subset relaxes towards the terminal model restricted to the subspace; the MLPL method effectively averages an estimate over these

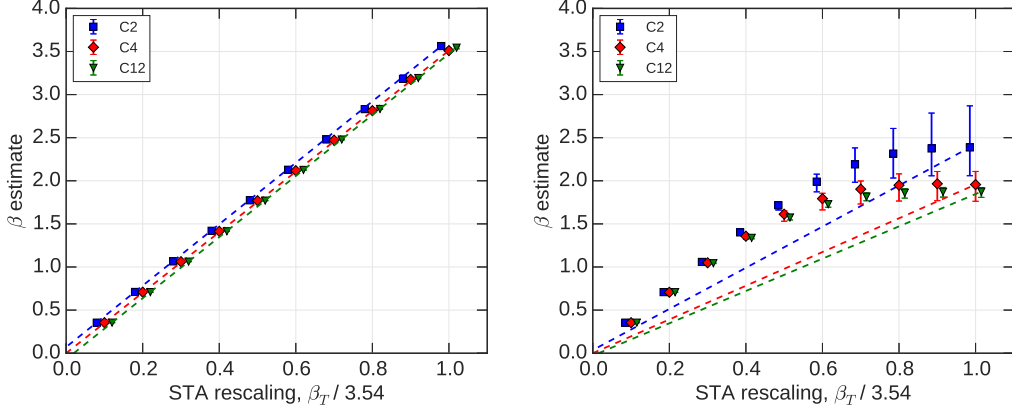


Figure 2: Bars represent quartiles over 100 instances of RAN1 at each scale, estimates for β for in each case 10^4 samples generated by STA. C2 and C12 data points are offset for visibility. (left) Temperature estimates by the MLPL method. The MLPL estimate for thermal annealers matches the terminal model at all scales. (right) Temperature estimates by ML. A non-linear trend is apparent due to ergodicity breaking, which is not captured by MLPL estimates.

subspaces. By contrast the ML estimate accounts in part for the distribution between modes, characterized at an early (higher energy) stage of the anneal that is better described by smaller inverse temperature. Note that the equilibrated distribution at the ergodicity breaking point is a quantum one for DW2X, unlike thermal annealers, so we ought to understand the deviation in the local and global temperatures in terms of the quantum parameterization $(\Delta(t), E(t))$ [13]. Still, the classical description in terms of β (2) provides the correct intuition.

Response curves such as these can be used to choose a suitable parameterization of the terminal model. If we know the β we are targeting then we can choose the terminal model (terminal β or rescaling parameter r) appropriately. In the absence of information on the objective at a global scale, a local information curve such as MLPL curve can be used as a compromise. It should be noted that the response curves will be a function of the problem type – in particular, inhomogeneity of couplings and fields can have a strong impact on the MLPL curve for DW2X. These curves could be the basis for the assumptions required by the multi-canonical method to move from an estimate of the β gap to estimates of β for each distribution independently. A study on the estimates of $\Delta\beta$ in the canonical method as a function of β_T and r are shown in Appendix E.1.

4.2 Single qubit freeze-out in DW2X

Figure 3(left) illustrates that local temperature, as measured by the MLPL method, is a non-linear function of the rescaling parameter. One can see that this temperature has only mild dependence on problem size (mild by comparison with the trend in ML). We illustrate this nonlinearity again in Figure 4, where we find the local temperature of a trivial single qubit model $H(x) = x$ for the DW2X under different fields (at various rescaling parameters r). This result can be compared with simulations of single qubit dynamics using the Redfield equation [36, 37]. Using the best estimate of the annealing schedule of the DW2X with a $20\mu\text{s}$ anneal time (described in Appendix B.2), and fitting a physical temperature parameter $T_{\text{phys}} = 20.5\text{mK}$ (in good agreement with the measured operational range), we are able to describe the non linearity very accurately.

The origin of this non-linear dependency is the freeze-out of individual qubit dynamics at the end of the annealing process [16, 13]. The MLPL method estimates temperature by looking at the pattern of excitations on single qubits, in the context of the sample from which they were drawn. In STA (and indeed in some simulations of quantum annealers - without physical dynamics) there is typically at least one update of all spins at the terminal temperature, so that within each sample spins are adjusted (locally) to the energy signal at the end of the anneal. This is the reason that the pattern of self-consistent spin excitations is consistent with β_T in STA, and the

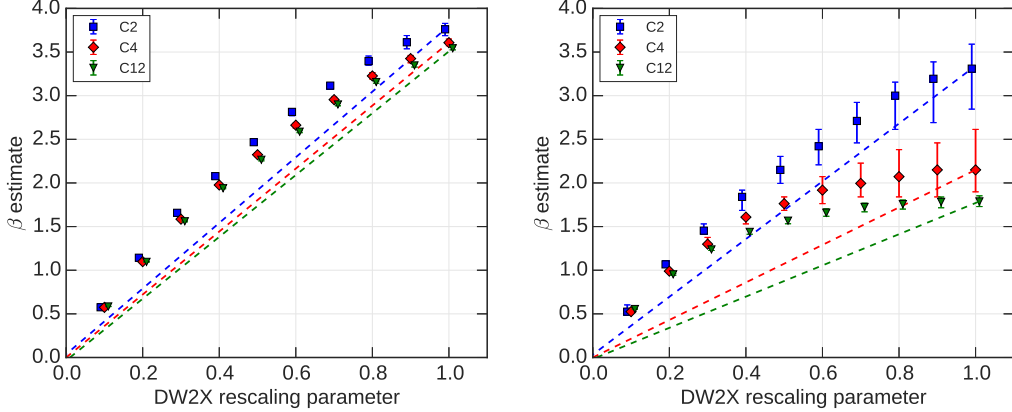


Figure 3: As per Figure 2, but using samples from DW2X. (left) The MLPL method is non-linear, unlike the STA results. (right) The maximum likelihood method shows qualitatively similar features to STA. Note that the C12 result for the MLPL estimate at $r = 1$ is identical to that in figure 2, the STA parameter β_T was chosen to meet this criteria as discussed in Appendix B.1.

MLPL estimator indicates $\beta \approx \beta_T$ for any β_T . In physical quantum annealers, where the rate of transitions is controlled by the transverse field which changes throughout the anneal; the dynamics are fundamentally different. Since the transverse field becomes very small before the terminal energy scale is reached, the state of the qubit is controlled by the Hamiltonian operator at this intermediate point in the anneal.

Even though quantum dynamics as simulated by the Redfield equation are complex in the case of a single qubit, there is a very simple explanation for the shape of the effective temperature curve. Assuming that late in the anneal the physical temperature is negligible in the single qubit dynamics, the transition rate for single qubits is known to be determined exclusively by the ratio $\alpha(s) = \frac{E(s)}{\Delta(s)}$, where $E(s)$, $\Delta(s)$ are the envelope functions described in Appendix B.2. We determine from the Redfield simulation with rescaling parameter $r = 1$ the single qubit dynamics freeze-out at $s^* = 0.65$ (or $13 \mu\text{s}$ during an anneal of $20 \mu\text{s}$). This means that the single qubit distribution reflects a locally equilibrated distribution at $\alpha^* = \alpha(s^*)$. The effective inverse temperature describing this point will be proportional to the energy scale $E(s^*)$. Now if we submit the problem under a new rescaling parameter $r < 1$, freeze-out will happen at a later time $s(r)$ where $\alpha(s(r)) = \alpha^*$ and the effective inverse temperature will be proportional to $rE(s(r))$.

Figure 4 shows good agreement between this single qubit freeze-out effective temperature and the Redfield simulation. Thus in the case of a single qubit the non-linear dependence of effective temperature on the rescaling parameter is determined by the annealing schedule.

4.3 Implications of the single qubit result for other ensembles

We can extend the concept of single qubit freeze out so that it can describe patterns of local temperature via MLPL for general multi-qubit problems. We will appeal to a classical argument that appears to explain some features of the non-linearity, and differences amongst problem classes and system sizes. As described in Appendix C, the MLPL estimator is determined by examining the effective fields on individual qubits in sampled states

$$\zeta_i = h_i + \sum_j (J_{ij} + J_{ji})x_j . \quad (14)$$

At the single-qubit freeze-out point the dynamics of individual qubits will slow down, and the state will evolve according to a local field operator analogous to (14). If the neighbors of a spin take prescribed classical states, then the spin will evolve late in the anneal equivalently to a single qubit in a field. The MLPL estimator accumulates a signal from the pattern of excitations on all sites and

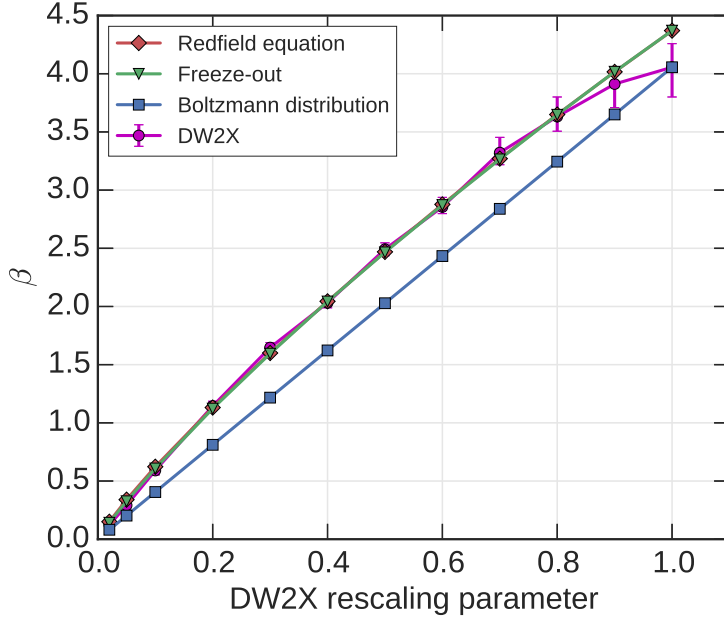


Figure 4: Single qubit β dependence on the rescaling parameter, for the single qubit Hamiltonian $H(x) = x_i$. We plot the DW2X median value together with 25-75 quantiles as error bars. Simulation of the physical dynamics gives the Redfield curve, and the “freeze-out” curve shows is based on the assumption of a single freeze-out point. In a system that is equilibrated at the end of the anneal a linear dependence would be expected.

in every sample, and smaller (but non-zero) values of $|\zeta_i|$ contribute most significantly to this signal. For a given problem there is a distribution of $|\zeta_i|$ so a single curve such as Figure 4 is insufficient. However, we may anticipate the result as a weighted average of such curves that varies only slightly amongst problems of a given class. Concavity of MLPL curves is therefore to be expected, except where many $|\zeta_i|$ are small (but non-zero) and we are in the near-linear regime of the curve 4.

From our samples, we can approximate separately a value of ζ_i for every variable, in every sample, late in the anneal. In the RAN1 problems ($h_i = 0$, $J_{ij} = \pm 1$) only a limited set of integer values for ζ_i are possible. For $|\zeta_i| = 1$, the qubit had a freeze-out characterized by the inverse temperature for $r = 1$ in Figure 4. However, the majority of non-zero local fields will be larger ($|\zeta_i| \geq 2$), and these freeze-out even earlier (at smaller β). The MLPL estimate will merge these values, so that we find something intermediate. A simple explanation for the trend of decreasing β with system size in Figure 2(left) would therefore be that we see fewer instances of $|\zeta_i| = 1$ relative to $|\zeta_i| \geq 2$; this is indeed the case.

In the AC3 problem couplings J_{ij} take values $\pm 1/3$ and ± 1 and effective fields will often be as small as $|\zeta_i| = 1/3$. These qubits freeze-out significantly later than the RAN1 counterparts, and so are characterized by larger MLPL estimates of β . This is consistent with the observed pattern in Figure 17(left) that AC3 MLPL β estimates are larger than those for RAN1, are weakly dependent on system size and have approximately linear scaling with r . This is discussed further in Appendix G, where AC3 results are presented.

The MLPL estimator ($\hat{\beta}_{MLPL}$) merges the estimates coming from sizes of large $|\zeta_i|$ with those of small $|\zeta_i|$. However, we can build locally-consistent estimators to tease apart contributions. For example, it is valid to define an estimator to separately consider excitations over even connectivity sites ($\hat{\beta}_{even}$) where the smallest non-zero $|\zeta_i|$ is 2, and odd connectivity sites ($\hat{\beta}_{odd}$) where the smallest non-zero $|\zeta_i|$ is 1. These estimators agree up to statistical error in STA, or drawing perfect samples, but in DW2X $\hat{\beta}_{even} < \hat{\beta}_{MLPL} < \hat{\beta}_{odd}$. We have found similar trends in studying ensembles with special connectivity distributions [14]. This is precisely the kind of local deviation that can be cleaned up by post-processing.

King et al. have previously noted that the distribution of effective fields, and by extension the degree distribution in RAN1 problems, can have a significant impact on the late anneal quantum dynamics [14]. Our explanation is purely classical, but seems to explain the trends with respect to problem classes and problem sizes quite well. However, at this stage we cannot rule out a role for multi-qubit freeze-out quantum phenomena in MLPL estimation.

4.4 The mean square error estimator

The mean square errors on correlations associated to the DW2X and thermal annealers for a typical instance of RAN1, and a typical instance of AC3, are shown for the C12 (1100 variables) problem size in Figure 5. Though there is significant variation between the curves associated to different instances of these models, we chose amongst 100 random instances exemplars that were representative of the point (β, MSE) at which the DW2X curve is minimized.

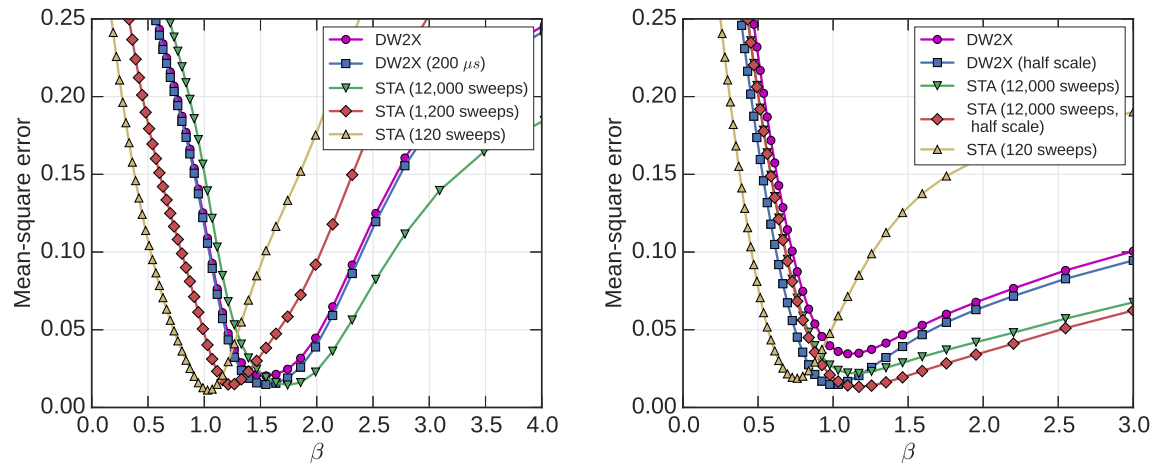


Figure 5: Both STA and DW2X can be used to sample from a RAN1 problem with small errors over an intermediate range of β . Objective performance is shown for two typical instances under several annealer operating conditions. (left) Results for the AC3 exemplar. (right) Results for the RAN1 exemplar. Standard errors determined by jack-knife methods are negligible compared to the marker size. To avoid clutter we show only variation of the anneal time in the left figure, and only variation of the rescaling parameter ($r = 0.5$ in DW2X, $\beta_T/2$ in STA) in the right figure.

Both STA and DW2X performance is best characterized at intermediate β values. If we halve the terminal temperature or rescaling parameter we can further improve the objective behavior, except perhaps at very large values for β , as is shown for the RAN1 exemplar. If we anneal for longer, we also improve the objective value of the distributions at low and intermediate temperatures, as shown for the AC3 exemplar. Annealing for longer is expected to allow equilibration to lower temperatures, and so improves objective values. Annealing to a lower terminal model, by contrast, concentrates annealing resources towards the initial part of the anneal where dynamics are effective (rather than at the end of the anneal where ergodicity breaking has already occurred and cannot be mitigated). It also reduces the disjunction between the local and global distribution features.

Figure 7 shows the mean square error achieved at the point it is minimized, for a large set of C12 (1100 variable) problem instances. Ideally we wish for heuristics that are both sampling at large β and with small errors. Figure 6 shows the MMSE estimator in comparison to the ML estimator. These two estimates indicate different operational temperature ranges. The fact that the ML estimator is significantly larger may be related to the fact that it is very sensitive to the mean energy. The mean energy continues to decrease late in the anneal as samples sink towards their respective local minima (see Figure 1), whereas sinking towards a local minimum will have a relatively weaker impact on correlations once ergodicity breaking has occurred, and so MSE indicates a higher effective temperature. Phenomena such as the sinking towards local minima (and

the consequent effects on temperature estimation) are one reason we recommend post-processing as a tool to isolate macroscopic phenomena in Section 3.3.

By annealing with modified β_T or r , improvements are made for sampling intermediate or small β . By contrast, it is relatively hard to sample effectively from large values of β by modifying these parameters; additional time resources are required to make an impact. For this reason, we may argue that, generally, the larger the inverse temperature estimate, the more useful the annealer will be for hard sampling applications. However, it is important to note that an estimate for β , independent of the objective measure, may be risky or misleading. In Figure 6(right), the DW2X system at full scale indicates a lower MMSE β than the DW2X system operating at half scale. However, we can see that at this larger β value the half scale system is still more effective as a heuristic.

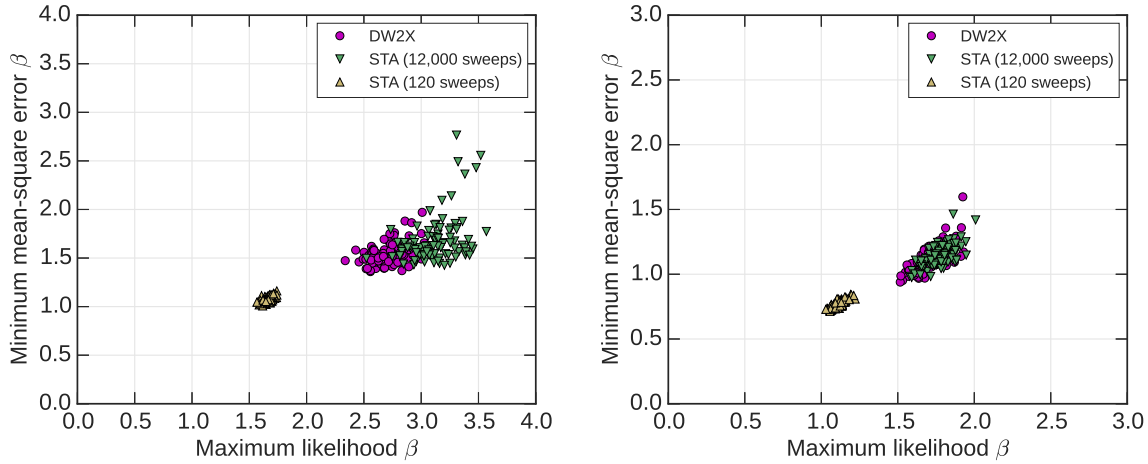


Figure 6: Statistics over the set 100 AC3 (left) and RAN1 (right) problems at C12 scales, as per Figure 7. MMSE and ML estimators of temperature give different, but strongly correlated, results. The ML estimate is typically larger, a partial explanation is the sinking of samples towards local minima late in the anneal, which through its impacts on mean energy has consequences for the ML estimate.

In this section we have presented the rather intuitive objective: mean square error on correlations, which we can evaluate with input from parallel tempering simulations. We have not presented the KLD objective behavior, since at C12 scale the estimators we wish to use are subject to strong bias as discussed in Appendix F. In that appendix we also show that where the KLD objective can be approximated, in smaller systems, it shows a similar qualitative trend.

4.5 Effectiveness of post-processing

In Sections 4.1 and 4.4 we demonstrated how adjusting anneal duration, or the terminal temperature, can allow better objective outcomes. In this section we consider briefly the effect of post-processing by one sweep of blocked Gibbs as discussed in Section 3.3. This post-processing changes dramatically the local distribution of samples, hence the MLPL estimate. However, the KLD and MSE objective, and the temperatures minimizing these objectives, are affected by a combination of the local and global distribution and so are modified in a non-trivial way by post-processing, except at small β where even simple post-processing is very powerful.

Figure 8 shows that MSE on correlations are, as expected, improved by post-processing. The improvements are dramatic in the regime $\beta \approx 0$, impressive over intermediate values of β , but almost negligible for larger β . This is because for larger β it is macroscopic distribution effects that dominate, and these are not strongly affected by a single sweep of blocked Gibbs. After post-processing, the MSE curve has two minima. There is no guarantee there should be two local minima working with arbitrary distributions. The first local minimum ($\beta = 0$) is evidence for the power of post-processing. Since one sweep of blocked Gibbs samples effectively at $\beta \approx 0$, independent of

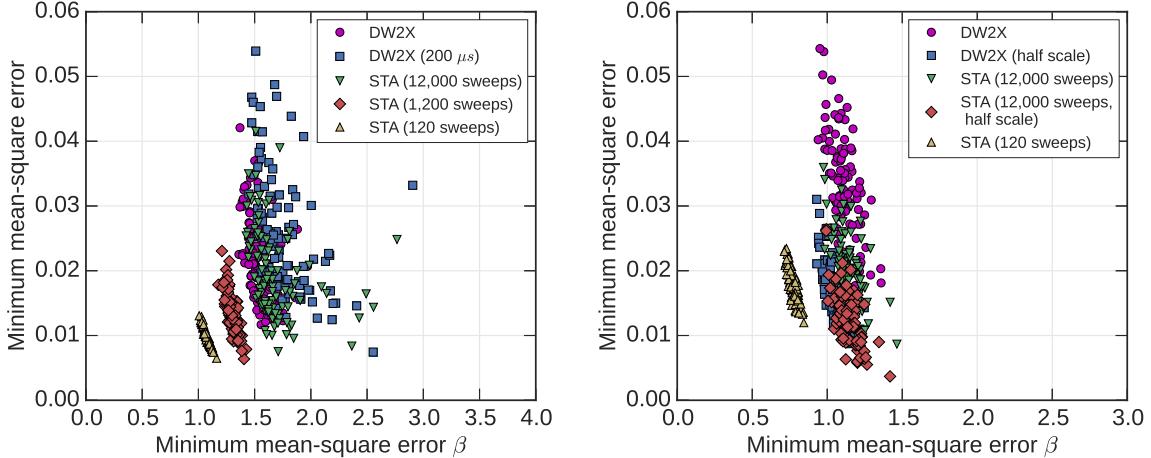


Figure 7: Statistics over the set 100 RAN1 (left) and AC3 (right) problems at C12 scales. Small objective values at large inverse temperatures are difficult to obtain, and so desirable in a heuristic sampler. Sampling effectively at small inverse temperature is less valuable (e.g., 120 sweep STA annealing). Modification of the annealing parameters significantly changes the distribution, allowing more effective emulation at some inverse temperatures. To avoid clutter we show only variation of the anneal time in the left figure, and only variation of the terminal model rescaling (r, β_T) in the right figure; the effects are qualitatively similar in each of these models at C12 scale.

the initial condition $P_A, \beta = 0$ will be a global minimum for any heuristic distribution. The second local minimum appears due to the closeness (at the macroscopic level) of the annealing distribution to some particular low-temperature Boltzmann distribution, a sweet spot of operation that may be of practical interest. A further example of this sweet spot behavior is shown in the context of the KLD objective in Appendix F.

This local minimum is not much changed relative to the raw distribution for this problem, and as we apply more powerful post-processing it may be expected to move to slightly smaller β . Post-processing reduces the error everywhere, but more so at smaller β . If the post-processing allows global redistribution of samples we may anticipate the disappearance of the local maximum separating the “easy for post-processing regime” from the “good for this annealer” regime; at which point a best operational regime for the annealer is less clear. However, we can assume that powerful post-processing of this kind is too expensive in the types of multi-modal problems where annealers are useful.

Figure 9 shows the statistics for the local minimum mean square error estimator, and its relation to the local maximum likelihood estimator, to be compared against Figure 6 that has no post-processing. The local minimizer is the unique local minimum of the post-processed curve (see Figure 8), which indicates the good operating regime. A global minimum is always at $\beta = 0$, but this is not of interest.

In Figure 9(left) we see that, relative to the distribution without post-processing, there is a slight shift leftwards in all distributions, and significant shift downwards that appears approximately proportional to the MSE without post-processing. The effect of local relaxation is to give the impression of better estimation at low temperature. Here the effect is partially lifted to reveal that the macroscopic distribution may be characterized by slightly smaller β .

In Figure 9(right) we see how the MMSE estimate decreases in all annealers, but by a less significant amount than the downward trend in the ML estimator. The two remain strongly correlated under post-processing. It is natural to expect that the local relaxation, which shifts samples towards their local minimum, may have a bigger impact on KLD than MSE, because it is easy to raise the energy by post-processing which impacts ML in a systematic manner, but it is difficult to redistribute samples macroscopically, which may be required to alter MMSE.

The particular effects demonstrated on the exemplar instances of Figure 9 are reflected at the

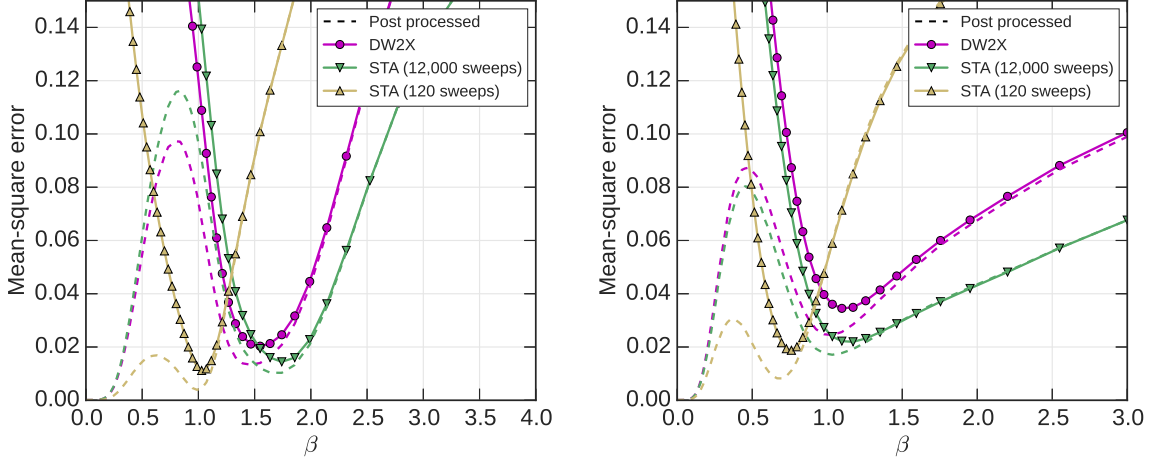


Figure 8: Simple forms of post-processing can have a quantitatively large effect on objectives at small and intermediate temperatures. The C12 problem exemplars consistent with Figure 5 are shown. At low β a single sweep of blocked Gibbs can completely correct all errors. At high β there is relatively little effect, however the effect is significant in the intermediate range of inverse temperature where the annealers can be considered most effective.

distribution level in Figure 10.

5 Discussion

In this paper we have considered several temperature estimators applied in the context of a physical quantum annealer set up for optimization (DW2X), and a standard simulated thermal annealer (STA). We have demonstrated how different objective measures of closeness to the Boltzmann distribution respond differently to local and global distribution features. An important phenomenon we observe is that in annealing distributions we have a range of temperature estimates according to the method employed. We have shown that estimators indicating larger temperature are those responsive to macroscopic (global) features of the distribution. From an estimator perspective we have *global warming*: the more effective the estimator is in capturing global distribution features the higher the temperature that is typically indicated. Ergodicity breaking qualitatively explains the origin of this phenomenon in annealers, both DW2X and STA.

Local distributional features, which are well characterized by a temperature, are easy to estimate by self-consistent methods. We showed both single distribution and multi-canonical forms of self-consistency. Self-consistent approaches work from the data, and could be adapted to correct for biases in the distribution. The main problem with such methods is that they may indicate a good fit on the basis of incomplete (or biased) information about the distribution. In particular, if a heuristic fails to see a representative set of modes in the distribution, it is unlikely to discover this self-consistently. Thus even if the bias over the observed set can be corrected, the distribution may still be bad with respect to Boltzmann distribution.

The local approximation method is able to capture an important difference between quantum and simulated annealers related to the speed of physical dynamics. This can be identified in the non-linear dependence of the local temperature estimate to variation of the DW2X rescaling parameter. Quantum simulations on single qubits provide an explanation for this phenomenon.

Describing the global distribution in terms of temperature(s) is more tricky; we proposed KLD and MSE as measures of deviation from the Boltzmann distribution, and based on these objectives developed estimators for the best temperature. Each of these objectives is affected in slightly different ways by deviations locally and globally from the Boltzmann distribution. The ML estimator is typically more strongly affected by the local distribution than the MMSE estimator, and therefore typically returns a larger estimate of inverse temperature. To remove the local distribution effects

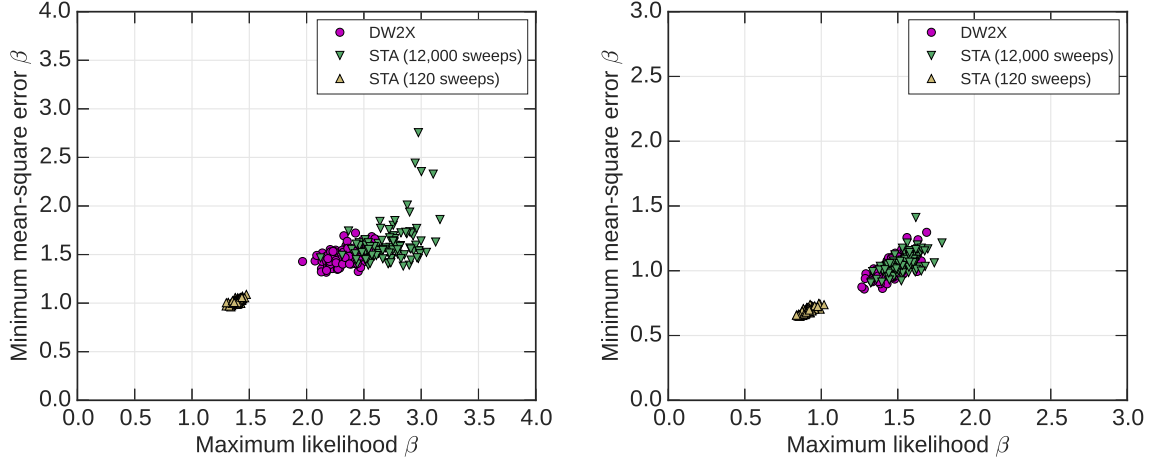


Figure 9: As per Figure 6, but now all distributions are modified by one sweep of blocked Gibbs sampling. The estimators for inverse temperature are reduced, as the effect of the local distribution (characterized by larger inverse temperature) is partially removed.

we have proposed to take the initial distribution and apply local post-processing in order to isolate the macroscopic distribution effects that are truly a limitation on practical performance. Applying some degree of post-processing may also be valuable in practice, in particular for DW2X since the post-processing is strictly classical and complementary.

We emphasize that because efficient post-processing allows significant manipulation of the local temperature, we consider this temperature not particularly important in practical applications. If we post-process, the post-processing temperature itself will be synonymous with the local temperature; the local temperature need not be measured.

Important ideas incidental to the main thread are discussed in Appendices. These include a consideration of the effect of embedding on the distribution of samples in Appendix I, the development of an effective estimator for the Kullback-Leibler divergence in Appendix F, a consideration of spin-reversal transformations to mitigate sampling error in the DW2X in Appendix H, and an experiment to test how “local” our definition of local temperature actually is in Appendix D.

At various points in this paper we have included results both for STA and DW2X. We have briefly discussed timing considerations in Appendix B: all the STA results we present, if generated with state of the art algorithms with a single thread, would require more time per sample than the anneal time of DW2X ($20\mu s$). This is assuming the 6.65ns per bit flip achievable for ± 1 valued couplings in [38]. However, our intention is not to make a performance comparison, which is beyond the scope of this work. It is interesting that, despite the fact that the DW2X annealer has been designed and tuned for optimization, it produces good statistics at intermediate temperature ranges, and that the more powerful STA methods we study show a qualitatively similar behavior. Each annealer type can be substantially improved with small parameter modifications, and it is reasonable to expect that more significant modifications to the annealing schedule would likely yield improvements in both cases.

When considering the value of annealers in inference problems, it is also important not to forget a variety of other powerful inference methods that may achieve a similar objective. In particular, simple variations on STA such as annealed (or population) importance sampling methods and other multi-canonical MCMC methods can often be tailored to the graphical structure of the problem under investigation [39, 40, 7, 41, 35, 42].

While two particular objectives (KLD and MSE) have been considered in this paper, the objective should generally be tailored to the application. One quite generic objective choice not considered is $KLD[B_\beta, P_A]$, the KLD with the ordering of distributions reversed (3). It is connected to the log-likelihood of Boltzmann samples under P_A . If we are very close to a Boltzmann distribution, this will behave similarly to (3), the form we have evaluated. Outside of this regime the former

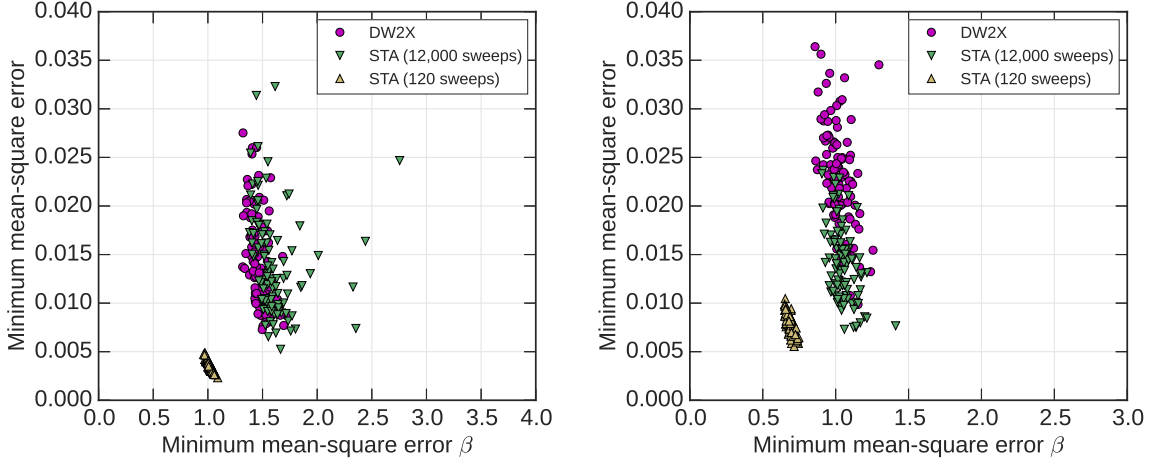


Figure 10: As per Figure 7, but with distributions modified by one sweep of blocked Gibbs sampling. Objectives are improved everywhere very significantly, and by a comparable fraction across the different annealers.

objective is in many ways preferable. In particular, it is more sensitive to features such as missing mass (poorly sampled sections of the solution space) and is expected to indicate a temperature range more sensitive to global rather than local distribution deviations. Unfortunately, there are many technical challenges to using such an objective, and the criteria for minimization are rather complicated. We therefore settled on mean square error on correlations, and $\text{KLD}[P_A, B_\beta]$.

From the perspective of both errors on correlations and KLD, the balance of evidence certainly indicates that there is potentially a sweet spot for application of either STA or DW2X to sampling. This sweet spot may be tuned, to a degree, by modification of the annealing parameters, and more importantly, by post-processing. However, evaluation of this sweet spot is difficult to do self-consistently, and someone interested in applications may have to undertake hard work to discover (and have confidence in) annealer performance. Having available curves such as those in Section 4.1, probably for some weakly post-processed distribution, would allow parameters of the annealer to be set optimally. It may seem computationally intensive (defeating the value of the heuristic) to evaluate the macroscopic distribution before using an annealer, but it is reasonable to assume that for some classes of problems at large scale, the local and global temperature properties will be common across the class. In other time-dependent applications of annealers the statistics of the distributions being learned change slowly, so that only periodic evaluations of the temperatures may be required.

An important potential application of quantum annealers is in machine learning [12, 11], where other heuristic samplers (not annealers) are prevalent. A common heuristic used in machine learning is called contrastive divergence (CD) [43, 44]. B_β is approximated in CD by taking the ground truths (a set of training examples) and evolving them by an MCMC procedure. This is an example of the post-processing scheme used and recommended in this paper, except that annealed samples are replaced by the ground truths. Like the annealing distribution, the distribution of training examples may be incorrect in both its local and global features, the effect of the MCMC procedure is to tidy up local distribution deviations. After post-processing the distribution is used directly - in effect the post-processing temperature is taken to be correct³, without consideration of potential macroscopic deviations. The success of this algorithm in practice indicates that learning procedures may be quite tolerant of macroscopic deviations from the Boltzmann distribution in application provided the local temperature is correct. This would be good news since it may be computationally expensive to quantify macroscopic deviations, but it is easy to measure and manipulate local temperature in annealers.

One feature of D-Wave quantum annealers that might lead us to consider a different approach

³In machine learning we can take the post-processing temperature to be $\beta = 1$, without loss of generality.

is the quantum part, as already discussed. The single qubit freeze-out, and dynamical slow-down at larger scales, are described by quantum models. The quantum Boltzmann distribution may be a better fit to sample sets drawn from the DW2X, and perhaps in “post-processing” we should think of the quantum space as the target, rather than the classical one. This is certainly a promising direction for future work.

6 Acknowledgments

The authors are grateful to Andrew King, Cathy McGeoch and Kevin Multani for their help in experimental design and method analysis. We also thank Alejandro Perdomo-Ortiz and John Realpe-Gómez for input regarding their multi-canonical method.

References

- [1] A. Sinclair and M. Jerrum. Approximate counting, uniform generation and rapidly mixing markov chains. *Information and Computation*, 82(1):93 – 133, 1989.
- [2] G. F Cooper. The computational complexity of probabilistic inference using Bayesian belief networks. *Artificial intelligence*, 42(2):393–405, 1990.
- [3] P. M. Long and R. Servedio. Restricted Boltzmann machines are hard to approximately evaluate or simulate. In *Proceedings of the 27th International Conference on Machine Learning (ICML-10)*, pages 703–710, 2010.
- [4] R. Salakhutdinov and G. Hinton. Deep Boltzmann machines. In *Proceedings of the International Conference on Artificial Intelligence and Statistics*, volume 5, pages 448–455, 2009.
- [5] T. Kadowaki and H. Nishimori. Quantum annealing in the transverse Ising model. *Phys. Rev.E*, 58:5355–5363, Nov 1998.
- [6] S. Kirkpatrick, C. D. Gelatt, and M. P. Vecchi. Optimization by simulated annealing. *Science*, 220(4598):671–680, 1983.
- [7] D. P. Landau and K. Binder. *A Guide to Monte Carlo Simulations in Statistical Physics*. Cambridge University Press, Cambridge, UK, 2nd edition, 2005.
- [8] Z. Bian, F. Chudak, W. G. Macready, and G. Rose. The Ising model: teaching an old problem new tricks. D-Wave Publications, available at <http://www.dwavesys.com/>, 2010.
- [9] M. Denil and N. de Freitas. Toward the implementation of a quantum RBM. In *NIPS 2011 Deep Learning and Unsupervised Feature Learning Workshop*, 2011.
- [10] V. Dumoulin, I.J. Goodfellow, A. Courville, and Y. Bengio. On the challenges of physical implementations of RBMs. In *Proceedings of the 28th AAAI Conference on Artificial Intelligence.*, 2015. arXiv:1312.5258v2.
- [11] M. Benedetti, J. Realpe-Gómez, R. Biswas, and A. Perdomo-Ortiz. Estimation of effective temperatures in a quantum annealer and its impact in sampling applications: A case study towards deep learning applications. arXiv:1510.07611, 2015.
- [12] M. H. Amin, E. Andriyash, J. Rolfe, B. Kulchytskyy, and R. Melko. Quantum boltzmann machine. arXiv:1601.02036, 2016.
- [13] M. H. Amin. Searching for quantum speedup in quasistatic quantum annealers. arXiv:1503.04216, 2015.
- [14] A. D. King, E. Hoskinson, T. Lanting, E. Andriyash, and M. H. Amin. Degeneracy, degree, and heavy tails in quantum annealing. arXiv:1512.07325, 2015.
- [15] J. King, S. Yarkoni, M. M. Nevisi, J. P. Hilton, and C. C. McGeoch. Benchmarking a quantum annealing processor with the time-to-target metric. arXiv:1508.05087, 2015.
- [16] M. W. Johnson, M. H. S. Amin, S. Gildert, T. Lanting, F. Hamze, N. Dickson, R. Harris, A. J. Berkley, J. Johansson, P. Bunyk, E. M. Chapple, C. Enderud, J. P. Hilton, K. Karimi, E. Ladizinsky, N. Ladizinsky, T. Oh, I. Perminov, C. Rich, M. C. Thom, E. Tolkacheva, C. J. S.

Truncik, S. Uchaikin, J. Wang, B. Wilson, and G. Rose. Quantum annealing with manufactured spins. *Nature*, 473(7346):194–198, May 2011.

[17] V. S. Denchev, S. Boixo, S. V. Isakov, N. Ding, R. Babbush, V. Smelyanskiy, J. Martinis, and H. Neven. What is the computational value of finite range tunneling? arXiv:1512.02206, 2015.

[18] M. J. Wainwright and M. I. Jordan. Graphical models, exponential families, and variational inference. *Found. Trends Mach. Learn.*, 1(1-2):1–305, 2008.

[19] C. J. Geyer and E. A. Thompson. Constrained monte carlo maximum likelihood for dependent data. *Journal of the Royal Statistical Society. Series B (Methodological)*, 54(3):657–699, 1992.

[20] E. L. Lehmann and G. Casella. *Theory of Point Estimation*. Springer texts in statistics. Springer, 2nd ed edition, 1998.

[21] G. Bresler, D. Gamarnik, and D. Shah. Hardness of parameter estimation in graphical models. arXiv:1409.3836v2, 2014.

[22] J. Besag. Statistical analysis of non-lattice data. *Journal of the Royal Statistical Society. Series D (The Statistician)*, 24(3):pp. 179–195, 1975.

[23] A. Montanari. Computational implications of reducing data to sufficient statistics. *Electron. J. Statist.*, 9(2):2370–2390, 2015.

[24] B. B. Bhattacharya and S. Mukherjee. Inference in Ising models. arXiv:1507.07055, 2015.

[25] J. Albert and R. H. Swendsen. The inverse ising problem. *Physics Procedia*, 57:99 – 103, 2014. Proceedings of the 27th Workshop on Computer Simulation Studies in Condensed Matter Physics (CSP2014).

[26] E. Aurell and M. Ekeberg. Inverse Ising inference using all the data. *Phys. Rev. Lett.*, 108:090201, Mar 2012.

[27] H. C. Nguyen and J. Berg. Mean-field theory for the inverse Ising problem at low temperatures. *Phys. Rev. Lett.*, 109:050602, Aug 2012.

[28] A. Perdomo-Ortiz, B. O’Gorman, R. Biswas, and V. N. Smelyanskiy. Determination and correction of persistent biases in quantum annealers. *Scientific Reports*, 6:18628, 2016.

[29] M. Mezard and A. Montanari. *Information, Physics, and Computation*. Oxford University Press, Inc., New York, NY, USA, 2009.

[30] T. F. Rønnow, Z. Wang, J. Job, S. Boixo, S. V. Isakov, D. Wecker, J. M. Martinis, D. A. Lidar, and M. Troyer. Defining and detecting quantum speedup. *Science*, 345(6195):420–424, 2014.

[31] H. G. Katzgraber, F. Hamze, and R. S. Andrist. Glassy Chimeras Could Be Blind to Quantum Speedup: Designing Better Benchmarks for Quantum Annealing Machines. *Phys. Rev. X*, 4:021008, Apr 2014.

[32] A. Douglass, A. D. King, and J. Raymond. *Theory and Applications of Satisfiability Testing – SAT 2015: 18th International Conference, Austin, TX, USA, September 24-27, 2015, Proceedings*, chapter Constructing SAT Filters with a Quantum Annealer, pages 104–120. Springer International Publishing, Cham, 2015.

[33] M. R. Shirts and J. D. Chodera. Statistically optimal analysis of samples from multiple equilibrium states. *The Journal of Chemical Physics*, 129(12), 2008.

[34] K. Hukushima and K. Nemoto. Exchange monte carlo method and application to spin glass simulations. *Journal of the Physical Society of Japan*, 65(6):1604–1608, 1996.

[35] A. Selby. Efficient subgraph-based sampling of Ising-type models with frustration. arXiv:1409.3934, 2014.

[36] K. Blum. *Density matrix theory and applications; 3rd ed.* Springer Series on Atomic Optical and Plasma Physics. Springer, Berlin, 2012.

[37] U. Weiss. *Quantum dissipative systems*. World Scientific, Singapore, 1993.

[38] S. V. Isakov, I. N. Zintchenko, T. F. Rønnow, and M. Troyer. Optimised simulated annealing for Ising spin glasses. *Computer Physics Communications*, 192:265 – 271, 2015.

- [39] R. M. Neal. Annealed importance sampling. *Statistics and Computing*, 11(2):125–139, 2001.
- [40] K. Hukushima and Y. Iba. Population annealing and its application to a spin glass. *AIP Conference Proceedings*, 690(1):200–206, 2003.
- [41] F. Hamze and N. de Freitas. From fields to trees: On blocked and collapsed mcmc algorithms for undirected probabilistic graphical models. In *Proc. Uncertainty in Artificial Intelligence*, 2004.
- [42] Z. Zhu, A. J. Ochoa, and H.G. Katzgraber. Efficient cluster algorithm for spin glasses in any space dimension. *Phys. Rev. Lett.*, 115:077201, Aug 2015.
- [43] G. Hinton. Training products of experts by minimizing contrastive divergence. *Neural computation*, 14(8):1771–1800, 2002.
- [44] M. Á. Carreira-Perpiñán and G. E. Hinton. On contrastive divergence learning. In *AISTATS*, 2005.
- [45] I. Hen, J. Job, T. Albash, T. F. Rønnow, M. Troyer, and D. A. Lidar. Probing for quantum speedup in spin-glass problems with planted solutions. *Phys. Rev. A*, 92:042325, Oct 2015.
- [46] A. D. King, T. Lanting, and R. Harris. Performance of a quantum annealer on range-limited constraint satisfaction problems. arXiv:1502.02098, 2015.
- [47] Z. Zhu, A. J. Ochoa, S. Schnabel, F. Hamze, and H.G. Katzgraber. Best-case performance of quantum annealers on native spin-glass benchmarks: How chaos can affect success probabilities. *Phys. Rev. A*, 93:012317, Jan 2016.
- [48] P. Bunyk, E. M. Hoskinson, M. W. Johnson, E. Tolkacheva, F. Altomare, A. J. Berkley, R. Harris, J. P. Hilton, T. Lanting, A. J. Przybysz, and J. Whittaker. Architectural considerations in the design of a superconducting quantum annealing processor. *IEEE Transactions on Applied Superconductivity*, 24(4):1700110, 2014.
- [49] D. Venturelli, S. Mandrà, S. Knysh, B. O’Gorman, R. Biswas, and V. Smelyanskiy. Quantum optimization of fully connected spin glasses. *Phys. Rev. X*, 5:031040, Sep 2015.
- [50] A. Janson, T. Luczak, and A. Rucinski. *Random Graphs*. John Wiley & sons, New York, NY, USA, 2000.
- [51] J. Cai, B. Macready, and A. Roy. A practical heuristic for finding graph minors. arXiv:1406.2741, 2014.
- [52] K. Bart. Bidirectional associative memories. *IEEE transactions on systems, man, and cybernetics*, 18(1):49–60, 1988.
- [53] T. Tanaka, S. Kakiya, and Y. Kabashima. Capacity analysis of bidirectional associative memory. In *Proc. Seventh Int. Conf. Neural Information Processing, Taejon, Korea*, volume 2, pages 779–784. Citeseer, 2000.
- [54] F. Yoshihara, K. Harrabi, A. O. Niskanen, Y. Nakamura, and J. S. Tsai. Decoherence of flux qubits due to $1/f$ flux noise. *Phys. Rev. Lett.*, 97:167001, Oct 2006.
- [55] R. Harris, M. W. Johnson, S. Han, A. J. Berkley, J. Johansson, P. Bunyk, E. Ladizinsky, S. Govorkov, M. C. Thom, S. Uchaikin, B. Bumble, A. Fung, A. Kaul, A. Kleinsasser, M. H. S. Amin, and D. V. Averin. Probing noise in flux qubits via macroscopic resonant tunneling. *Phys. Rev. Lett.*, 101:117003, Sep 2008.
- [56] S. Boixo, T. Albash, F. M. Spedalieri, N. Chancellor, and D. A. Lidar. Experimental signature of programmable quantum annealing. *Nature Communications*, 4, June 2013.
- [57] L. Paninski. Estimation of entropy and mutual information. *Neural Comput.*, 15:1191–1253, 2003.
- [58] P. Grassberger. Entropy Estimates from Insufficient Samplings. *ArXiv Physics e-prints*, July 2003.
- [59] T. S. Jaakkola and M. I. Jordan. *Learning in Graphical Models*, chapter Improving the Mean Field Approximation Via the Use of Mixture Distributions, pages 163–173. Springer Netherlands, Dordrecht, 1998.

- [60] B. Efron. *The Jackknife, the bootstrap and other resampling plans.* CBMS-NSF Reg. Conf. Ser. Appl. Math. SIAM, Philadelphia, PA, 1982. Lectures given at Bowling Green State Univ., June 1980.
- [61] T. Lanting, A. J. Berkley, B. Bumble, P. Bunyk, A. Fung, J. Johansson, A. Kaul, A. Kleinsasser, E. Ladizinsky, F. Maibaum, R. Harris, M. W. Johnson, E. Tolkacheva, and M. H. S. Amin. Geometrical dependence of the low-frequency noise in superconducting flux qubits. *Phys. Rev. B*, 79:060509, Feb 2009.

A Four standard DW2X compatible models

In this paper we investigate multiple families of Ising spin problems of the form (1). A number of exotic problem classes have been studied in the context of DW2X [45, 46, 14, 47]. Many of the motivations for these classes relate directly to optimization, and involve manipulation of the *very* low energy landscape. It should be noted that many of these manipulations do not lead to particularly interesting variations in the finite temperature behavior (of which we are more concerned), except perhaps for small system sizes. As an example it is understood that all Chimera structured models with independent and identically distributed couplings will show the same finite temperature behavior, and no finite temperature spin glass transition [31]. Our model choices are chosen with the aim of demonstrating strong and varied ergodicity breaking effects at the scales studied. This appendix describes the models studied and the motivation for their selection; beyond the set described we have considered some other unpublished classes and found similar phenomena.

The Chimera graph topology is shown in Figure 11, and must be respected in any problem sampled directly by DW2X [48]. It can be seen that qubits are arranged in tiles, each tile is a $K_{4,4}$, a bipartite graph of 8 qubits. Due to manufacturing errors, some qubits and couplings are defective and cannot be programmed.

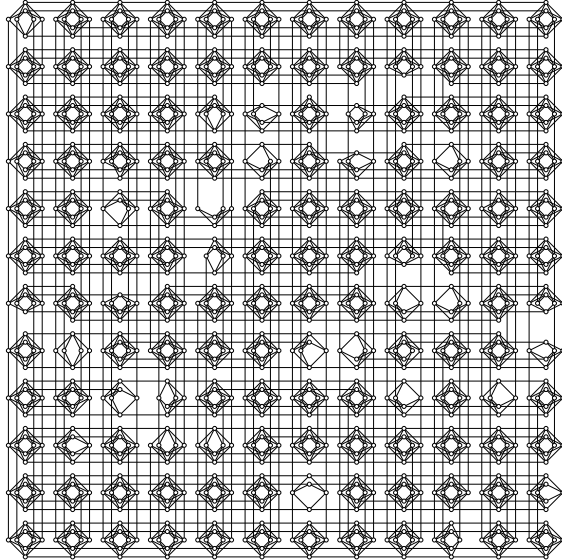


Figure 11: Working graph of the DW2X used; the topology is called Chimera.

- **Spin Glasses on Chimera graphs RAN1**

A simple spin-glass model in the context of DW2X experiments has zero fields ($h_i = 0$), with independent and identically distributed couplings uniform on $J_{ij} = \pm 1$, subject to the Chimera graph topology. These problems are called RAN1 [15]. Recent work has indicated that for some algorithms RAN1 may be a relatively easy problem in which to discover optima [30], and that asymptotically there is no finite temperature spin-glass phase transition [31], calling into question its usefulness as a test of scalable performance. Nevertheless, the problem class continues to demonstrate interesting phenomena in the context of quantum annealers and competing software.

We consider these problems defined over a square subgrid of the DW2X graph, we will call the Chimera subgrid CL , where L is linear dimension, the number of cells per row (and per column). Problems are studied at three scales: C2 (32 variables) as either C4 (127 variables on a square cell grid), or C12 (1100 variables), on a square cell grid. Inference on the former problems is possible by dynamic programming, the latter only by MCMC procedures.

- **Anti-Cluster Spin Glasses on Chimera graphs (AC3)**

In the AC3 models we consider all couplings to be distributed uniformly at random $J_{ij} = \pm 1/3$ inside the Chimera unit tiles, and set to a ferromagnetic values $J_{ij} = -1$ between cells [15]⁴. By making couplings relatively stronger between cells, longer range interactions are induced through sequences of strongly correlated vertical, or horizontally, qubits.

If the relative strength is chosen to scale appropriately with system size [49], then at sufficiently low temperature we would expect the vertical couplings and horizontal inter-cell couplings to energetically dominate the other couplings, and for each sequence of horizontal or vertical qubits to behave coherently as a single “chain” or logical qubit. The system would become equivalent to an embedded fully bipartite Sherrington-Kirkpatrick (SK) model.

We work with small Chimera graph sizes and an intermediate coupling ratio (3), the model then represents an interesting departure from RAN1 due to the increased long-range interactivity, but falls short of the embedded SK model paradigm. Another interesting point of variation from RAN1 is the small increase in precision (we use an alphabet $\pm 1/3$ and ± 1 in place of ± 1), which has consequence for the local estimation of temperature and single qubit freeze-out phenomena. As per RAN1, problems are on C2, C4, or C12 scale.

- **Random Not-all-equal-3SAT, NAE3SAT**

Random Not-All-Equal-3SAT (NAE3SAT) are a particular family of satisfiability problems closely related to 3SAT, and sharing the same computationally challenging features [29, 32]. We consider problems with N variables and $M = 1.8N$ clauses. Each clause m is described by 3 literals: a triplet of indices $\eta_{m,1}, \eta_{m,2}, \eta_{m,3}$ and a triplet of signs $a_{m,1}, a_{m,2}, a_{m,3}$ (a sign $-1/+1$ indicates a negative/positive literal). In random NAE3SAT, literals are selected independently: sampling uniformly the indices on $\{1, \dots, N\}$, and the signs on ± 1 . In the models we generate we apply the further restrictions that (a) all problems we consider are satisfiable, (b) every variable appears in some clause and (c) all variables are dependent (the graph is connected). The configuration model can be used for sampling these topologies [50].

An Ising model in which the ground states of energy 0 are coincident with the satisfying assignments of NAE3SAT (true/false maps to $+1/-1$), and other states are assigned an energy equal to the number of clause violations, is described by the Hamiltonian

$$H(x) = \frac{1}{4} \sum_{m=1}^M [a_{m,1}a_{m,2}x_{\eta_{m,1}}x_{\eta_{m,2}} + a_{m,1}a_{m,3}x_{\eta_{m,1}}x_{\eta_{m,3}} + a_{m,2}a_{m,3}x_{\eta_{m,2}}x_{\eta_{m,3}} - 1] \quad (15)$$

By expansion, we find the form (1) up to an unimportant constant offset. Finding ground states of this Hamiltonian solves an NP-complete satisfiability problem. However, the solution space structure at non-zero (but low) energies is also interesting in its own right when $M \gtrsim 1.5N$, paradigmatic of hard to sample from energy landscapes [29]. This hardness is due to the existence of a finite temperature random first order phase transition [29, 7].

The process of embedding can be used to generate an auxiliary problem that preserves the ground state properties, but is solvable by the DW2X system [51]. Data is only presented for the 40 variable instances of the NAE3SAT problem. The number of qubits required to represent the embedding problems fluctuates, and is determined automatically by the embedding procedure, but typically fits comfortably on a subgraph of the 8 by 8 cell (C8) Chimera graph. Inference on the unembedded problem is typically possible by dynamic programming, whereas inference in the embedded problem requires MCMC.

Embedding, and transforming the samples obtained back into the logical space, can have important consequences for temperature estimation, as discussed in Appendix I. The NAE3SAT problem is also used to demonstrate variation amongst locally-consistent estimators in Appendix D.

- **A bidirectional associative memory (BAM) model**

The bidirectional associative memory model is a neural network model without hidden units. It is the bipartite generalization of the Hopfield model [52]. In the model studied here, a set of N

⁴We could equivalently assign the couplings between cells to ± 1 at random, due to a simple symmetry the problem is not meaningfully changed.

Ising spins are divided into two equal groups that are conditionally independent, and a set of M memories $\{\epsilon^{(m)}\}$ are drawn each independently and uniformly from $\{-1, +1\}^N$. If the model is trained to recall these memories under Hebbian learning, the learning procedure converges upon a distribution described by the Hamiltonian

$$H(x) = -\frac{2}{N} \sum_{i_1=1}^{N/2} \sum_{i_2=N/2+1}^N x_{i_1} x_{i_2} \sum_{m=1}^M \epsilon_{i_1}^{(m)} \epsilon_{i_2}^{(m)}. \quad (16)$$

A similar model might be learned by regularized Boltzmann machine learning of the same set of patterns.

The BAM model has an easy to understand energy landscape when the number of memories to be stored is small compared to the number of variables N [53]. For large enough N and $\beta > 1$ the Boltzmann distribution is defined by $2M$ well defined *modes* (these modes come in pairs related by a trivial symmetry). The memories $\pm \epsilon^{(m)}$ define the centers of these modes, and are local ground states (up to perhaps a small Hamming distance). This is a nice model for theoretical exploration since there is a clear distinction between the global features (modes), and local features. To be solved on DW2X (for more than 8 variables) the model would need to be embedded, but in this paper we only apply STA to this model. A 128 variable, $M = 3$ memory, model is studied in Appendix E.2 to demonstrate interesting features of a multi-canonical approximation.

B Annealer dynamics and parameterization

The distributions we analyze describe either samples generated by a simulated thermal annealing (STA) procedure, or by the DW2X quantum annealer. Annealing dynamics are described, and we discuss how the schedules for annealing are defined, and chosen for optimization applications.

B.1 Blocked Gibbs sampling and simulated thermal annealing

Blocked Gibbs is a standard Markov chain Monte Carlo procedure closely related to the Metropolis algorithm procedure [7, 44]. To understand blocked Gibbs we must first assume a graphical model, such as Figure 11, in order to identify conditionally independent variable sets [18]. A heuristic graph coloring will reveal conditionally independent sets of variables, in general it is fast to find some graph coloring. In a bipartite graphical model (e.g., the RAN1, AC3, or BAM models of Section A) there is a unique pair of such sets. The conditional probability distribution on each set is a factorized distribution. We can resample each spin x_i in the set \mathcal{S} , setting its value according to probability

$$P_\beta(x_i | x \setminus x_i) = \frac{\exp(-\beta \zeta_i(x) x_i)}{2 \cosh(\beta \zeta_i(x))}, \quad (17)$$

where $\zeta(x) = (J + J^T)x + h$. We proceed through the sets in a fixed order, for each set resampling all variables – this procedure is called a sweep. This procedure can be iterated at a fixed temperature, and the distribution of samples is guaranteed to approach the Boltzmann distribution parameterized by β over sufficiently many sweeps.

The blocked Gibbs sampling procedure at large β is not very efficient in sampling for multi-modal distributions, since samples are immediately trapped by the nearest modes (which may be of high energy), and escape only over a long time scale. A more effective strategy for multi-modal problems is blocked Gibbs annealing, in which β is slowly increased towards the terminal value β_T with a sequence of sweeps (choosing a schedule, i.e. an assignment of sweep numbers to temperatures). In this paper we consider an annealing schedule that is a linear interpolation between 0 and β_T .

Given the linear schedule, a generic implementation of STA has two parameters: the total anneal time, and the terminal inverse temperature β_T . Unless stated otherwise we will base our evaluations on 10^4 samples, and these samples are all independent and identically distributed (within the limitation of the strong pseudorandom number generators we use). If STA equilibrates throughout the anneal, it will approach a Boltzmann distribution parameterized by β_T , whereas if ergodicity

breaking plays a role, we expect it to be characterized by a smaller value that depends on the objective applied. We now explain how anneal times and β_T were chosen in this paper:

B.1.1 Parameterization of STA

We apply STA to the BAM model, choosing $\beta_T = 4$ and 200 as the number of sweeps. The inverse temperature is chosen so as to be well above the known thermodynamic phase transition [53], so that samples are well separated into modes. The number of sweeps is taken as 200 so that in the STA distribution we observe large frequencies over many of the lowest energy states, in order that we may evaluate the multi-canonical method of Benedetti et al. without modification [11].

In the main section we study a set of problems using both DW2X and STA, for the RAN1 and AC3 problem classes. Due to controversy surrounding comparison of these two algorithms, we were more careful in these choices [30, 38, 15]. A principled choice for DW2X operating parameters would be ones that minimize “Time to Solution” (TTS), an optimization criterion, as discussed in Section B.2. We find that $20\mu s$ anneals minimize this quantity for the DW2X.

For STA, we present results for $\beta_T = 3.54$ for RAN1, and $\beta_T = 4.82$ for AC3. We choose the STA parameter β_T so that the distribution of local excitations in STA and DW2X are comparable; we make the two solvers similar in their *local* properties, so that differences between the annealers reflect more interesting *global* features. To achieve this the STA parameter β_T is chosen equal to the MLPL estimate of β at full scale for DW2X (see Figure 3). An alternative interesting choice for β_T would be to minimize TTS. While this would also be principled, we finally opted against this choice. In the case of RAN1 our choice $\beta_T = 3.54$ is not too dissimilar to the value ($\beta = 3$) that had been previously been proposed for optimization applications [15, 30, 38].

To find the number of sweeps to use in STA, we minimize TTS in the median instance. For RAN1 we determined a rule of thumb the held across all problem sizes in this paper: number of sweeps = $1000L$, i.e., for a C12 graph 12000 sweeps are used. We applied this same rule of thumb to AC3 problems.

A second choice for the number of sweeps is to match the time per sample of DW2X. A recent efficient implementation of the Metropolis algorithm for ± 1 valued couplings achieves a rate of 6.65 spin flips per nano-second [38]. In C12 problems we have 1100 active qubits, and so $20\mu s$ would allow for $\frac{20000 \text{ ns}}{1100 \text{ spin flips}} * 6.65 \text{ spin flips/ns} \approx 120$ sweeps (updates of all variables).

In all RAN1 and AC3 experiments we chose to present the $1000L$ sweep data. For some C12 problems we also show the equalized time-per-sample result of 120 sweeps, along with a value intermediate (on the exponential scale) of 1200 sweeps.

B.2 DW2X sampling

In the case of the DW2X, the annealing is controlled by a time-dependent transverse field $\Delta(t)$ and an energy scale $E(t)$. These quantities are shown in Figure 12 for the DW2X system used in this paper. The physical temperature (T) of the system varies with time and load on the device and is difficult to estimate. We have experimentally observed a physical temperature which is 22.9 in the median, with quartiles of 22.0 mK and 25.6 mK, over the data taking time period. We did not analyze the time scales associated to temperature fluctuations in depth, but much of the variation occurs on long time scales, so that in a single experiment we typically found a tighter range of temperatures applied. The unitless Hamiltonian operator in effect at any point in the anneal is given by

$$\hat{H}(s) = \frac{\hbar}{k_B T} \left(\frac{\Delta(s)}{2} \sum_i \sigma_x^{(i)} + \frac{E(s)r}{2} \left[\sum_{ij} \frac{J_{ij}}{\max(\{|J_{ij}|\}, |h_i|)} \hat{\sigma}_z^{(i)} \hat{\sigma}_z^{(j)} + \sum_i \frac{h_i}{\max(\{|J_{ij}|\}, |h_i|)} \hat{\sigma}_z^{(i)} \right] \right) \quad (18)$$

where $s = t/t_{max}$ is the rescaled time, and the coefficient \hbar is Planck’s constant. The Hamiltonian parameters can be considered rescaled to maximum value 1, this is the meaning of the denominator $\max(\cdot)$. r and t_{max} are the rescaling parameter and the anneal time parameter, respectively. Throughout this paper, we adopt the convention that the Hamiltonian for the problem is fixed, and treat r the rescaling r to be a parameter of the heuristic (DW2X). In current operation of the DW2X

system, this manipulation is achieved in practice by turning off autoscale, and manually rescaling the values of $\{J_{ij}, h_i\}$ submitted. We find the convention of modifying the quantum Hamiltonian (18) to be more intuitive than considering modification of the classical Hamiltonian that is submitted: when we rescale downwards we are implying the use of smaller energy scales $E(t)$ in the annealer, we anticipate that β is reduced.

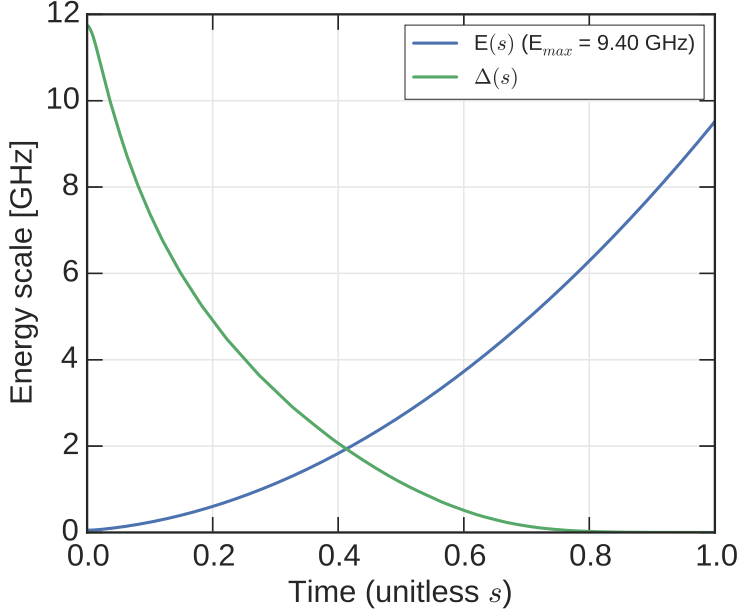


Figure 12: The DW2X operational energy scales during the anneal.

Proceeding (infinitely) slowly, so that equilibration occurs at the terminal model, we would be guaranteed to sample a diagonalized state described by a Boltzmann distribution (2) coincident with the classical Hamiltonian (1). Equating the prefactors for the two unitless Hamiltonians we have $\beta_0 = hE_{max}/(2k_B T) = 11.3$, which is the terminal inverse temperature – the expected overall scaling of the Hamiltonian. In Section 4.2 it is discussed why we do not equilibrate at this inverse temperature, and why the inverse temperature we do find is not necessarily a linear function of the rescaling parameter r .

A number of noise sources affect the components of the processor, aside from temperature fluctuations. These have been increasingly mitigated with each generation of D-Wave processors and by calibration efforts, but remain significant in the processor used [9, 46, 54, 55]. A simple model for the combined effect of error sources is one of independent zero-mean Gaussian distributed offsets on each programmed field and coupling; fitting this model to data for simple Hamiltonians estimates for the variance of 0.05^2 for fields, and 0.035^2 for couplings have been established in some systems (relative to a programming range of $[-1, 1]$ for J and $[-2, 2]$ for h) [14, 49, 10]. Such a model can provide intuition for the scale of noise, and the precision available to programmers; but does not account for time dependence in the noise sources, some systematic errors, and cross talk.

For purposes of this exposition we will ignore time-dependence in the samples except in the treatment of Appendix H, and approximate our samples drawn from DW2X as independent and identically distributed. Our batches of samples are generated, unless otherwise stated, by collecting 10^4 samples split across 10 programming cycles. This is a standard collection procedure that trades off quality of samples against timing considerations – including annealing time, programming time and read-out time. The programming cycles exploit spin-reversals, a noise mitigating technique that strongly suppresses correlations between programming cycles [56], see Appendix H for a description of spin-reversals and their impacts.

In this paper we consider only two embedded problems experiments, relating to the NAE3SAT problem with 40 variables. These are in Appendices D and I. When we sample from an embedded

problem we obtain a distribution on the qubit states, not on the “logical states” of the original problem. We can create a distribution on the “logical space” problem by projecting samples into that space. The embedding we use in this paper utilizes chains to enforce identity relations amongst qubits, so that when chains are intact we are in a subspace that has a one-to-one mapping in energy back to the logical space problem. Samples in this subspace can be converted directly into samples on the logical problem, and if the distribution is Boltzmann on the embedded space, it will be Boltzmann on this subspace (thereby the logical problem), and with the same parameter β .

Samples that violate these chains may be numerous, and can be brought into the chain-intact subspace by error correction methods (these can be thought of as post-processing in the embedded space). Most naive amongst these methods is chain voting (assigning all values in a chain to the value most represented in the chain). This is the only form of projection evaluated in this paper – more sophisticated projecting methods would involve a more careful study of the difference in the energy landscapes and perhaps a consideration of quantum chain dynamics.

B.2.1 Parameterization of DW2X

Our criteria for selection of the default rescaling parameter r and the anneal time is minimization of the “Time to Solution” (TTS) [15, 30, 38]. TTS is the expected time required to see a ground state for the first time. For the three problems studied with DW2X, it is optimal to choose a minimal programmable anneal time ($20\mu s$), and a maximum programmable energy scale $r = 1$. A second (and not uncorrelated) reason to use these parameters is that they are the default operation mode of the DW2X annealer. Since we are attempting to minimize some other objective, TTS is not necessarily the optimal way to use the DW2X heuristic in these two parameters.

C Maximum log-pseudo-likelihood

Maximum log-pseudo-likelihood (MLPL) is an attempt to replace the maximum likelihood estimator by a tractable one [22, 24]. This is a common heuristic in parameter estimation, although it is more commonly applied for larger parameter sets, as a stand in for Boltzmann machine learning procedures.

The pseudolikelihood estimate might be achieved by the following substitution for $P_\beta(x)$ in (3)

$$P_\beta^{PL}(x) = \prod_i B_\beta(x_i | x \setminus x_i) \quad (19)$$

and minimizing with respect to β . This method can be justified by its results, and rederived in other ways, but is sometimes difficult to interpret – notably (19) is not a probability.

Maximum likelihood estimation requires the NP-hard to calculate quantity of mean energy. Pseudo likelihood allows us to bypass this hard inference task. One way to think about the additional power of pseudo-likelihood is that it uses additional information from every sample, not just the essential statistic, energy - which is all that is used in a maximum likelihood estimate[26, 23].

As discussed Section 3.1 we can derive the same estimate for β from the energy matching criterion (4) averaging over all possible single bit-flip resamplings (10). This provides a clear interpretation for the method, and presents natural generalizations. In the case of the pairwise Ising model $H(x) = x^T J x + h^T x$, the MLPL estimate is given by $EM(\beta) = 0$, where

$$EM(\beta) = \sum_{x \in \mathcal{S}} \sum_i x_i \zeta_i(x) \frac{\exp(2\beta x_i \zeta_i(x))}{1 + \exp(2\beta x_i \zeta_i(x))} \quad (20)$$

and the vector $\zeta_i(x) = [h_i + \sum_j (J_{ij} + J_{ji})x_j]$ is the effective field. Note that $-2x_i \zeta_i$ is the energy change of flipping the state of spin i . Provided there exists at least one $\zeta_i(x) > 0$, and one value $\zeta_i(x) < 0$ (at least one local excitation in some sample), then this equation has a unique finite solution which can be found, for example, by a bisection search method.

D Extensions of the self-consistent approximation

The maximum log-pseudo-likelihood estimator is determined by the energy matching criterion under the self-consistent approximation (8), with single bit resampling (10). Our argument throughout this paper has been that all choices for W_β will likely lead to quantitatively similar *local* estimates of β , as they redistribute samples only locally and preserve macroscopic biases. In this appendix we demonstrate that the situation is slightly more blurred. One implementation of (8) in this Appendix is to take W to be a sequence of m sweeps of blocked Gibbs, and to solve the energy matching criterion under this sequence of increasingly powerful approximations. As m goes to infinity we would recover B_β perfectly, and so obtain the global estimate to inverse temperature, for small m the approximation is increasingly local as m decreases. MLPL is even more local than single-sweep, and so produces an even higher estimate to β .

In Figure 13 we demonstrate the inverse temperature estimates obtained as a function of the different self-consistency criteria (m). Results are for sampling of 100 random 40 variable NAE3SAT problems using DW2X; the samples are obtained by embedding the Hamiltonian and “chain-voting” the samples into the $N = 40$ dimensional logical space. In this way each of the 10^4 anneals yields a sample.

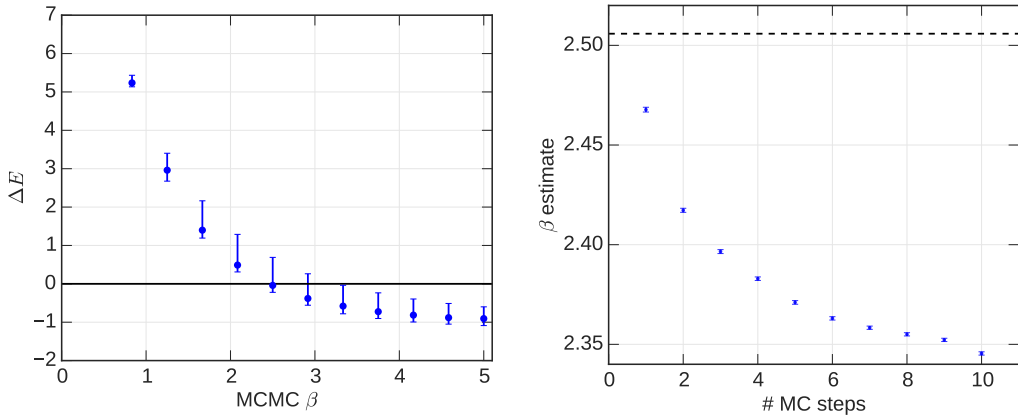


Figure 13: Median and quartiles over a set of 100 NAE3SAT problems (40 variables, clause-to-variable ratio of 1.8). (left) $\text{EM}(\beta)$, the deviation from the energy matching criterion (4) is shown as a function of β used in our one sweep of blocked Gibbs approximation to $B_\beta(x)$. When $\Delta E = 0$ we have an approximation to the maximum likelihood estimator. (right) Estimation of β using blocked Gibbs self-consistency as a function of increasing number of sweeps; as we move to larger number of sweeps we move towards the maximum likelihood estimate of β , and further from the MLPL estimate (shown as the dashed line).

In Figure 13(left) we show the energy matching value $\text{EM}(\beta)$ (4) for 100 different problem instances under $m = 1$ sweep of blocked Gibbs sampling approximation. Setting $\text{EM}(\beta) = 0$ we obtain the Maximum Likelihood estimate. In the Figure 13(right) we demonstrate how, as we increase the amount of post-processing m , the median estimate of β evolves downwards, towards the maximum likelihood estimate. Errors in Figure 13(right) represent uncertainty associated to the blocked Gibbs procedure itself, which was repeated many times per initial condition P_A . In the distribution over 100 instances there is significantly more variation.

We can see that self-consistent approximations can be improved and yield values closer to the maximum likelihood estimate (and further from the MLPL estimate) by increasing the power of the kernel W used in the post-processing method. This problem is however a very small one, of only 40 variables, and effects are less pronounced in larger hard problems.

E Estimation from multi-canonical methods

Two multi-canonical methods are explored experimentally in this paper: the self-consistent multi-canonical (SCMC) approximation introduced in Section 3.2, and the linear regression multi-canonical (LRMC) method of Benedetti et al. [11]. In this appendix we first discuss how multi-canonical methods may capture both local and global distribution features. We discuss limitations of multi-canonical methods, but also the fact that using the method in combination with MLPL can be used to efficiently indicate the presence of ergodicity breaking. We show in Appendix E.1 some results demonstrating $\Delta\beta$ estimation in RAN1 problems. The results show patterns similar to those for the single distribution methods, but interpretation is difficult due to the interaction between rescaling and ergodicity breaking. In Appendix E.2 we demonstrate the use of multi-canonical methods in isolating global and local effects. The choice of methods is not specific to the task in each subsection; we might leverage either method to achieve similar results in the respective sections.

Let us consider how two different annealer parameterizations may differ in distribution for STA with the SCMC method (assuming qualitatively similar arguments for DW2X, and for the LRMC method). Suppose two STA differ in the terminal inverse temperature, in one case annealing to $A_1 = \beta_0$ and in the other case to $A_2 = (1 - \epsilon)\beta_0$, for relatively small ϵ . With reference to Figure 1, we anticipate that both distributions are subject to a similar pattern of ergodicity breaking, but at the end of the anneal relax locally according to the different terminal inverse temperatures. The energy gap is a combination of energy gaps within each mode, and the energy gaps between modes. Restricting to replica-exchanges within the modes we may expect to see $\Delta\beta = \epsilon\beta_0$, but between modes of significantly differing energy, we would expect a much smaller value for $\Delta\beta$. If the energy gap between modes is large (as is the case schematically Figure 1) then the replica exchange probabilities between valleys will dominate the estimator, and we see a value close to zero. This is of course only one scenario, and depending on the relation between the rescaling and the ergodicity breaking we may see different patterns.

Since multi-canonical methods depend on both global and local features, we can infer ergodicity breaking by comparison with approximators that capture only local distribution features. We have two distributions and so can efficiently obtain MLPL estimates for each, as well as calculate $\Delta\beta$ by a multi-canonical estimate. Inconsistency of these estimates is an indicator of ergodicity breaking, but one which may be difficult to interpret independently of other knowledge about the distribution. This may be useful, but we caution that it cannot be relied upon to capture ergodicity breaking in general. Since it is self-consistent, and hence only sensitive to differences amongst observed modes, it will not capture ergodicity breaking related to the unseen modes (missing mass). This sensitivity to missing modes is a problem with all self-consistent estimation methods. Another way to see ergodicity breaking, or perhaps simply bias in the estimators, would be to consider three pairs of distributions (A_1, A_2, A_3) , measuring $\Delta\beta$ between each. Of course, this should yield a consistent set of gaps if we have a Boltzmann distribution and unbiased estimators for the gap.

We would like to note a limitation of the energy gap matching criterion (6). In order for the equation to be solved for some finite $\Delta\beta$ it is necessary that the range of the empirical distributions on energy overlap. Meaning, that the smallest energy of the hotter distribution is smaller than the largest energy on the colder distribution. In order to have low variance estimation we understand that the distributions ought to overlap strongly, otherwise the result is very sensitive to a small number of outliers in the energy distribution.

The LRMC method also has some shortcomings. Firstly, a linear regression method is employed. The objective being minimized, least squares, is not a particularly informative one and it is difficult to convert a fitting error to useful information about the quality of the distributions. Secondly, a necessary feature of the method is that pairs of energy states are well occupied, which is a stronger requirement than in the SCMC method. Finally, the data points used in the fitting are noisy, and since the noise model will (at least for those low-occupancy energy levels) be non-Gaussian, a bias in estimation can be expected. Binning data so as to modify and mitigate for the errors, and to create compatible occupied levels, may itself introduce bias.

Aside from this we reiterate that use of multi-canonical methods have some disadvantages. Neither of the two methods have in our opinion been sufficiently and robustly tested, although the LRMC method has been successfully applied in a machine learning context. Both methods are

consistent estimators, but bias and variance are poorly understood; perhaps a careful consideration of how to extract maximum information is required [33]. Also, the methods presented require collection of two sample sets (even if our interest is only in one parameterization) and an assumption on $\Delta\beta$ as a function of the annealer parameterization. The assumption that β is linear in the rescaling parameter is correct in the absence of ergodicity breaking; but based on analysis of Sections 4.1 and Appendix E.1 requires some careful consideration.

E.1 Rescaling dependence with the SCMC method

In this section we plot estimates to $\Delta\beta$ using the SCMC method. We study 100 RAN1 distributions under DW2X sampling at various scales. In Figure 14 we compare two distributions that differ by 0.1 (left) or 0.2 (right) in the DW2X rescaling parameter. If we have equilibration at the terminal model, we anticipate a linear correspondence between the rescaling parameter and the inverse temperature, $\beta(r) \propto r$, and so we would expect a constant value. There is a clear departure. We determine larger gaps for the simpler models (smaller rescaling parameters, and smaller system size). The estimate for $\Delta\beta$ is also a non-linear function; the sum of $\Delta\beta$ for two successive pairs separated by 0.1 in the rescaling parameter is not consistent with the estimate based on a single pair of models differing by 0.2. Note that the absence of data points for larger systems and smaller β is owing to the fact that the estimator is only usable when the energy distributions overlap, if the energy distribution support is disjoint $\Delta\beta$ is estimated as infinite. The energy distributions are also quite well separated for larger system sizes (C12), so that these results might be considered relatively unreliable. In multi-canonical methods, as already noted, the rescaling should be chosen adaptively to allow reasonable overlap of the energy distribution.

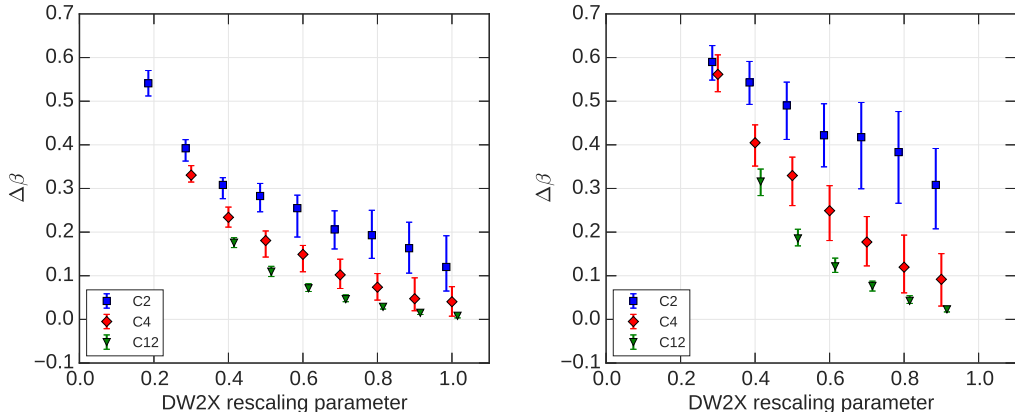


Figure 14: $\Delta\beta$ estimates in RAN1 models using the multi-canonical approach. Where points are absent the estimate is infinite due to non-overlap of the energy distributions at the different parameter settings. Error bars represent median and quartiles with respect to 100 instances studied. (left) 9 pairs of annealing distributions differing in the DW2X rescaling parameter ($r, r - 0.1$) were used, $r = 0.2, \dots, 1$. (right) 8 pairs of annealing distributions differing in the DW2X rescaling parameter ($r, r - 0.2$), $r = 0.3, \dots, 1$.

The details of these curves are difficult to interpret, but under the approximation $\beta(r) \propto r$ we do however see trends qualitatively consistent with those discovered based on ML and MLPL estimation in Section 4.1. Rescaling to small values of r we see larger inverse temperatures not far from the single qubit freeze-out prediction. For larger models we infer significantly smaller β values, indeed much smaller even than those predicted by the maximum likelihood method in the case of large systems. As outlined in this appendix, it may be expected that when the samples are dynamically trapped by modes with strongly differing energies, the estimate will approach zero.

E.2 Separation of global and local temperatures with the LRMC method

In this appendix we evaluate the LRMC method in the context of STA and the bidirectional associative memory model, described in Appendix A. We note that our implementation of Benedetti et al. is simplified relative to the most recent version of their paper, so that we utilize data less efficiently [11]. The model we evaluate has full bipartite connectivity, 128 variables, and 3 well separated pairs of modes (modes for a given pair are related by a change of sign of all Ising spins). We use sample sets of size 10^4 , generated at two different terminal β values ($A_1 : \beta_T = 4$ and $A_2 : \beta_T = 4x$, $x = 0.8$), in each case using a linear schedule in β of 200 sweeps.

To implement the LRMC method we first determine the energy that is most strongly represented in both sample sets. This *modal energy* E_m is typically the ground state energy for this model-annealer combination. We then find all other relevant energy levels E : here we select energies that appeared at least 10 times under both rescalings as relevant. This is because energy levels of low frequency are very noisy and we do not wish to introduce a noise model to complicate the story we present. If $\Omega_A(E)$ is the number of samples of energy e under a rescaling A then, assuming error bars are negligible, an estimate for β is obtained by a least square fitting of the curve

$$\log\left(\frac{\Omega_{A_1}(E)}{\Omega_{A_1}(E_m)}\right) - \log\left(\frac{\Omega_{A_2}(E)}{\Omega_{A_2}(E_m)}\right) = \beta(1-x)(E - E_m), \quad (21)$$

Solving for β , by linear regression, gives the estimator for distribution A_1 according to the LRMC method.

In our presentation of the LRMC method we will also implement a variation, fitting independently data on 3 different subspaces as well as the full space. Each E can be identified with one or more samples x , and we can cluster these E values according to which mode (memory) is best represented by x (up to symmetry, there will be only 3 modes). We plot all the data points in Figure 15, but color them according to this classification. As can be seen, the data in its entirety is not well described by a linear fit, but after clustering we see that a linear fit on each mode seems appropriate. Within each mode we can obtain a local temperature describing the distribution on that mode, that is as expected close to β_T . Despite the use of 10^4 samples, estimates are quite noisy due to the small sub-populations involved. Between the three curves there is a horizontal displacement: this reflects the fact that when we rescale the terminal β by a factor $x = 0.8$ there is no significant redistribution between the modes. This is expected since the ergodicity breaking happens early in the annealing procedure when the model is even further scaled down (approximately by 0.25, if we trust the large N behavior [53]), and so the two annealed distributions are macroscopically distributed between the modes in a similar manner. We can see how fitting all the data, as recommended by Benedetti et al., leads to a mixture of the global and local temperature [11].

We have shown that multi-canonical methods, in combination with clustering, yields additional information. A combination of local and global distribution features is apparent in this example, which is easy to establish since we chose the model to induce clusters that would be well defined and easy to discover. However, some of this information could be extracted with single-distribution methods. In particular, we see that the local temperature estimates have strong variation about the expected value $\beta_T = 4$ in the example presented. If by contrast we cluster the points and apply the MLPL estimator to each mode independently we obtain estimates of much lower variance based on the same number of samples. In this sense, MLPL seems to use the local information more efficiently than the version of the LRMC method we have presented.

F KLD estimation with mixture models on subspaces

The KLD (3) can be expressed as an entropy, a mean energy scaled by β , and a log partition term

$$KLD[P_A, B_\beta] = - \left[- \sum_x P_A(x) \log P_A(x) \right] + \beta \sum_x P_A(x) H(x) + \log(Z(\beta)). \quad (22)$$

We can determine a value of β minimizing this quantity through the energy matching criterion, but to understand quality we should evaluate this objective. An obvious problem is the evaluation of

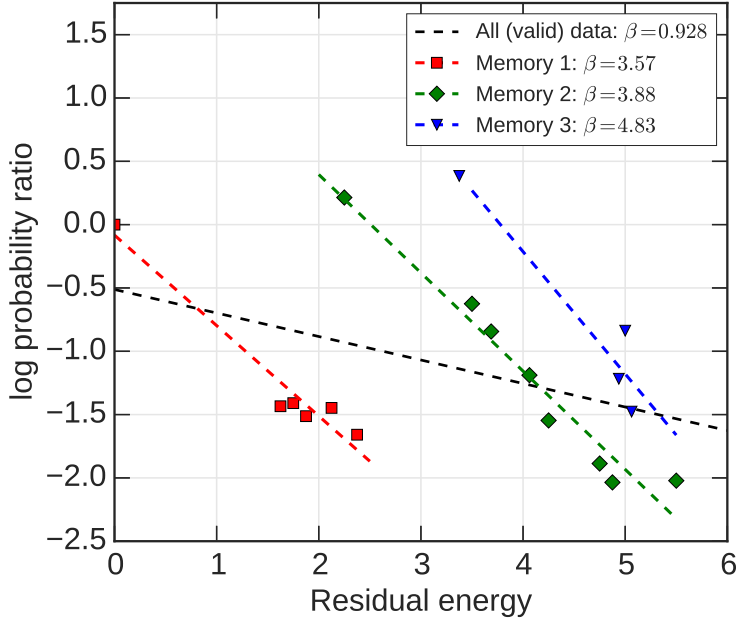


Figure 15: Log empirical frequency ratios are shown versus the residual energy (energy of the state minus energy of the ground state), the gradient characterizes a temperature. Energies are classified into modes by color, according to their nearest memory (Hamming distance). Each mode is well fitted by a single curve, which describes the local temperature and is in rough agreement with the target temperature, $\beta_T = 4$, as would be expected in STA. Between modes data are displaced horizontally. The three upper most points describe local ground states and do not show a decreasing trend – indicating that the rescaling by a factor $x = 0.8$ has little effect on the relative probabilities of local ground states relative to the global ground state. A linear fit to all the data gives a temperature that mixes this global distribution feature, with the contribution of the local estimates. A naive linear fit is made in each case, excluding analysis of errors on data points (errors on points grow moving rightward and downward, as state frequencies decrease).

$\log(Z)$, which is NP-hard. Nevertheless, methods such as annealed importance sampling or parallel tempering can be effectively employed for the problem types we have presented [19, 39].

Unfortunately evaluation of the entropy term from a set of samples is also problematic. Entropy is a non-linear function of P_A , and when estimated by plug-in type approaches (7) is subject to strong bias [57, 58]. The plug-in estimator based upon (7) yields a consistent estimator, but it is only when \log of the number of samples is greater than the entropy that we may accurately estimate the entropy term. Boltzmann distributions have entropy that grows linearly with the dimensionality. Thus, it seems that unless we make some strong assumption on the distribution P_A then we cannot capture the entropy term.

An example where we have such additional information is a post-processed distribution (13), which we have also argued in Section 4.5 of this paper provides more meaningful information on the practical usefulness of the samples obtained from annealing. If we evaluate the KLD for this distribution we can exploit knowledge of the analytical form for W_β to improve estimation, both the bias and variance of the crude estimator. The use of this analytical form can be interpreted as Rao-Blackwellization, with respect to the KLD of the post-processed distribution. It can also be shown that the KLD of the post-processed distribution provides a lower bound on the KLD for the unprocessed distribution, thus this quantity provides useful information on the unprocessed heuristic distribution.

We can develop this idea for blocked Gibbs post-processing of a bipartite Ising model. In a bipartite model, there are two sets of variables \mathcal{S} and \mathcal{T} , that are each conditionally independent (disconnected in the graphical model). If we first conditionally sample \mathcal{S} according to the Boltzmann distribution, and then \mathcal{T} , this is one sweep of blocked Gibbs sampling. The new set of samples are

described by a post-processed distribution (13) with the kernel

$$W(x|x') = B_\beta(x_S|x_T)B_\beta(x_S|x_T). \quad (23)$$

Evaluating the KLD for $P_{A,\beta}$ under this kernel, we are able to simplify the expression for the KLD to

$$KLD[P_{A,\beta}, B_\beta] = E \left[\log \left(\frac{P_{A,\beta}(x_S)}{B_\beta(x_S)} \right) \right] \quad (24)$$

where $E[\cdot]$ is an expectation with respect to $P_{A,\beta}(x_S)$. If we then take the plug-in estimator to the original annealing distribution P_A (7), we are able to approximate $P_{A,\beta}$ as

$$\hat{P}_{A,\beta}(x_S) = \sum_{x_T} \hat{P}_A(x_T) \prod_{i \in S} \frac{\exp(\beta \zeta_i(x_T) x_i)}{2 \cosh(\beta \zeta_i(x_T))} \quad (25)$$

where $\zeta(x) = (J + J^T)x + h$; $\zeta_i(x)$ is a function only of x_T for $i \in S$ due to the bipartite structure. The new expression (24) cannot be exactly evaluated in polynomial time, but perfect sampling from $P_{A,\beta}$ is possible. We can thus obtain an accurate estimate by evaluating the expectation by Monte Carlo sampling. Some tricks outlined in [59], who evaluate a similar functional form in the context of a different method, can be brought to bear in reducing this variance.

Two things have changed relative to estimating KLD with a plug-in estimator. Firstly, we are evaluating the KLD for distributions on a subspace S that is half as large as the original space $S \cup T$, secondly the distribution $P_{A,\beta}$ is not determined by a histogram on samples, but as a mixture of product distributions. Each of these features allows us to exponentially reduce (exponential in the dimensionality of the system, N) the number of samples required to accurately estimate KLD.

Using the estimator (24) we show results in Figure 16 for the KLD for a single typical instance from both RAN1 and AC3 problem classes at C4 scale (127 variable); there is strong variation between instances at this scale, but the two patterns are exemplars chosen to be typical in the maximum likelihood estimate for β . Solid lines indicate the estimator, and dashed lines indicate the jack-knife bias corrected estimate [60], the fact that the bias is appreciable even with 10^4 samples is an indication that we are approaching the limit of usefulness of this estimator. Indeed, the bias for the 40 sweep STA is so large as to render the estimate of entropy ineffective; the case of 400 sweeps is marginal, whereas for 4000 sweep STA and DW2X the estimates are accurate everywhere.

With 10^4 samples we would, in the absence of the post-processing trick, be limited to estimating KLD for distributions of entropy $\lesssim \log(10^4) = 9.4$; however, in this case we accurately measure entropy even as $\beta \rightarrow 0$ (where entropy is $128 \log(2)$). The KLD objective indicates strong performance at low temperature for DW2X, a reflection of the ability to reach consistently low energy scales [15]. If we instead used the MSE objective (5) across this range of β we find that STA performance is improved relative to DW2X.

Unfortunately, the use of this estimator is still fundamentally limited by the curse of dimensionality. To understand the limitations of this estimator we can consider first the best case scenario for performance, when the parameters $\zeta(x_T)$ happen to be optimal (minimizing the KLD). The KLD would then match that for a mixture of mean-field approximations [59]. In this context we can assert that the KLD for a single mixture component (derived from a single sample) can be no better than the mean-field approximation. The KLD of a mean-field approximation can be quite poor, except in the approximation of a single mode and the KLD between a mean-field approximation and many interesting Boltzmann distributions can be expected to grow linearly with the dimensionality. Also shown in [59], is the fact that the KLD decreases at most logarithmically in the number of mixture components (number of samples). In this scenario, we may still require a number of samples that is exponential in the dimensionality if we are estimating for a distribution that is close to a Boltzmann distribution.

This can be restated more informally. We know that a single sample processed by one sweep of blocked Gibbs may spread quite representatively over one mode of the distribution, and so capture local energy and entropy. However, if there are a large number of modes (including local minima which trap dynamics), then we need to see them all many times to begin estimating the inter-mode entropy term (also called complexity [29], capturing the distribution over modes) correctly. In the

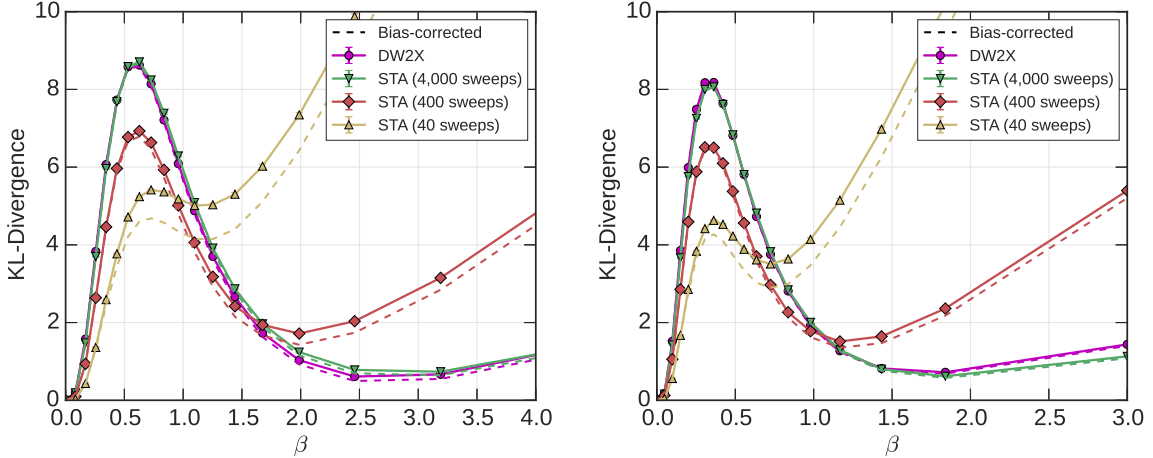


Figure 16: KLD results for two exemplar instances of AC3 (left) and RAN1 (right) each at C4 scale (127 variables). Full lines indicate the estimate, and the dashed lines indicate jack-knife bias corrected estimates. The variance determined by the jack-knife method is negligible by comparison with symbol size. The bias is very large for 40-sweep annealing, indicating we have insufficient samples to properly determine the KLD. Elsewhere we judge the bias not to significantly impact our conclusions.

case of RAN1 we find that quite quickly, beyond scale C4, the estimator can become strongly biased in a qualitatively similar manner to the plug-in estimator, particularly at intermediate temperatures; for this reason in the main text we have chosen MSE as our objective of choice.

G Estimating β in AC3 problems

In Figure 17 we show results from the DW2X for AC3 problems. In contrast to the RAN1 results in Section 4.1, here the MLPL method of estimating local β is much closer to the linear. The maximum likelihood estimator, however, still reflects the global distribution distortions due to ergodicity breaking. It is worth noting that both estimators show the DW2X to be sampling from colder temperatures than in the RAN1 case. Simulated thermal annealing results are not shown, since they would show the same features as in Section 4.1. We understand that higher precision problems may be expected to have MLPL estimates that scale linearly with the DW2X rescaling parameter, as discussed in Section 4.2.

H Impact of spin reversals on DW2X distributions

A spin reversal transformation of the Hamiltonian is defined by a random vector $\eta \in \{-1, 1\}^N$. Given such a vector we can define a new Hamiltonian

$$H_\eta(x) = \sum_{ij} J_{ij} \eta_i \eta_j x_i x_j + \sum_i \eta_i h_i x_i \quad (26)$$

Boltzmann samples drawn according to this distribution $\mathcal{S}_\eta = \{x\}$, can be transformed in Boltzmann samples on the original distribution, by componentwise multiplication of every sample by η . This is due to a symmetry. Any reasonable heuristic will respect such a transformation, thus the rule for Boltzmann samplers applies also to good heuristics in principle.

Although the DW2X is designed to obey this symmetry, it is weakly violated due to noise sources. Fortunately, spin-reversal transformations can be used to mitigate for the noise sources that cause this symmetry breaking. To do this, we can draw each sample according to a different spin-reversed Hamiltonian (26), transforming by a random vector η , and reversing this transformation to obtain

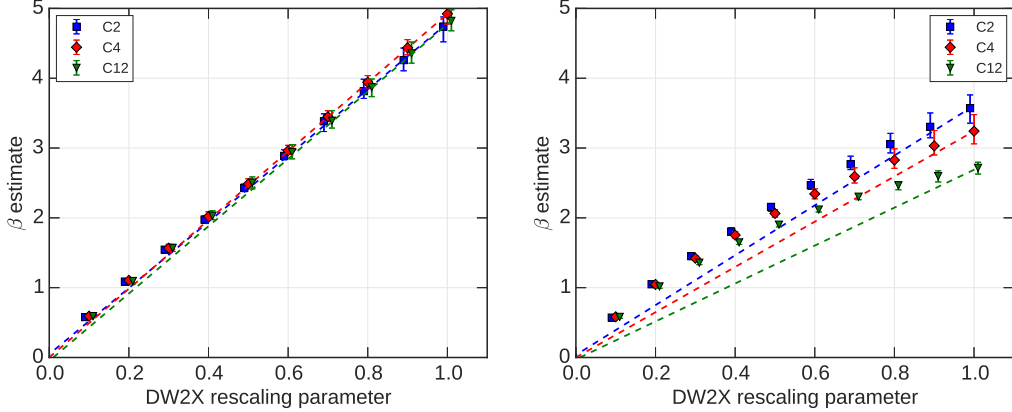


Figure 17: Bars represent quartiles over 100 random instances of AC3 at each scale. (left) Temperature estimates by the MLPL method. (right) Temperature estimates by maximum likelihood.

a sample in our original space. In this way, the random impact of noise on each representation is *averaged out* at the distribution level.

For purposes of our study, using many spin-reversal symmetries is also valuable in reducing autocorrelation of the samples. We find that whereas samples drawn sequentially for a fixed programming ($\eta = 1$) have some measurable autocorrelation that decays according to a $1/f$ spectrum [61]. The autocorrelation on statistics derived from samples that each differ by spin-reversal transformations is difficult to detect.

Unfortunately, it is currently very impractical to use a separate spin-reversal transformation for every sample, since each Hamiltonian submission must be programmed, requiring some time. It is more time efficient to draw samples in batches. In Figure 18 we show how the distributions err from the Boltzmann distribution as a function of the number of spin-reversals used in generating the sample set (total sample set size is normalized, so this uncertainty is removed). There is clearly a very large improvement in moving from sets constructed from one spin-reversal to sets constructed of 10 or more, but beyond this the returns are diminishing. For this reason we used for the bulk of our studies the more efficient format of 10 spin-reversals by 1,000 samples.

I Effects of embedding on temperature estimation

The process of projecting solutions from the qubit space into the logical space, required for solving non-Chimera structured problems (see discussion Appendix B.2), can have a significant impact on the distribution, and the temperature(s) that characterize the distribution.

We consider a single instance of a 40 variable NAE3SAT problem. This is an exemplar, but we do not intend for general conclusions to be drawn. For this instance the process of embedding transforms the Hamiltonian (16) on 40 variables into a Hamiltonian on 308 qubits⁵. The energy penalty per embedding violation is chosen to be 1.80 (in the unscaled units of (16)), reflecting a trade-off amongst various quantum annealing features (particularly precision). In other words, an embedding violating excitation is roughly twice as expensive as a clause violating excitation. When drawing 10^4 samples we see approximately 12.5% of samples are chain-intact, so that the majority of samples contain at least one embedding violation.

In Figure 19(left) we show the energy distribution of the samples in the 308 dimensional qubit space, evaluated according to the embedded Hamiltonian, and three Boltzmann distribution. We use parallel tempering to determine the mean energy and energy histogram for each of the Boltzmann distributions. In 19(right) we consider the energy distribution in the 40 dimensional logical space of the original problem for the subset of samples that were chain-intact, and for all samples (after

⁵We use the standard embedding function provided by the application interface for DW2X, based on the standard heuristic [51]. This embeds onto a C8 subgrid of the DW2X graph for the problem presented.

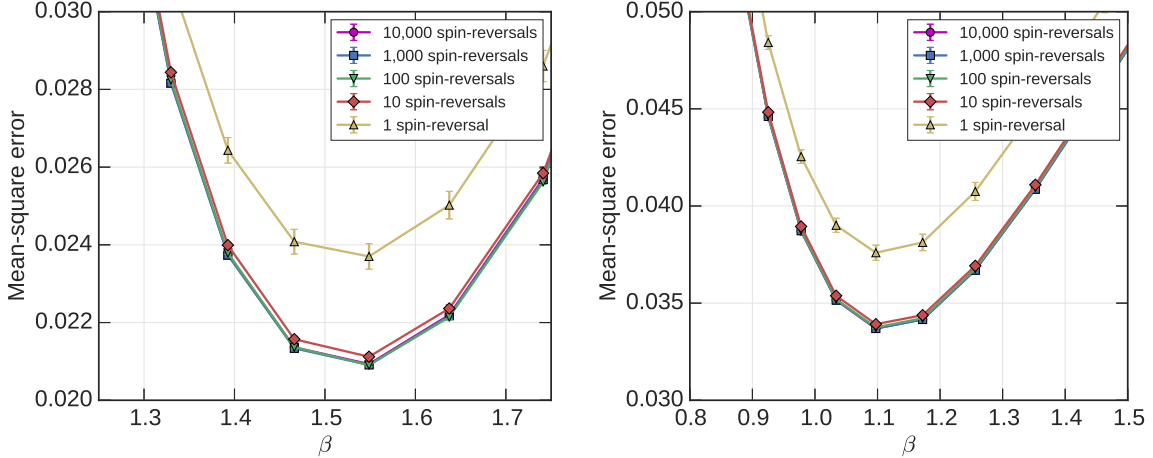


Figure 18: At C12 scale, spin reversals have a significant impact on MSE for both AC3 (left) and RAN1 (right). Given M samples, the error achieved by batch methods (m samples per spin-reversal with M/m spin reversals) is close to that of the ideal scenario of one sample per spin reversal, and converges rapidly as m decreases. The effect is a noisy one when few spin-reversal transformations are used, and is only statistically significant after averaging over many distributions (100 in this figure). We establish the mean estimate, and its standard error by bootstrapping of a sample set of 10000 spin-reversals sampling each time 1000 samples.

these are chain-voted into the lower dimensional space), as well as the same three Boltzmann distributions. The Boltzmann distributions were chosen by the maximum likelihood criteria with respect to the three hardware distributions that are plotted, and each distributions seem to be in qualitative agreement with some Boltzmann distribution – but not the same one. The error bars associated to the chain-intact distribution reflecting only the fact that we have fewer chain-intact samples from which to estimate. We use dynamic programming to determine the mean energy and energy histogram for each of the Boltzmann distributions. There is reasonable agreement of all three DW2X derived distributions with the energy spectrum of some Boltzmann distribution. However, we caution that this does not guarantee that the MSE on correlations, or some other statistic weakly dependent on the energy spectrum, will also be Boltzmann. We did not thoroughly test in this regard.

We can see that in the embedded problem the value of β that best describes the mean energy is relatively large. By contrast the estimate over the subspace where chains are intact is slightly smaller. Including chain-voted samples alongside the chain-intact samples decreases the β estimate on the subspace (we introduce relatively more high energy states). If the distribution is Boltzmann in the embedded space, then the same distribution (β) describes the chain-intact subspace, and therefore the logical problem on 40 variables. In this example (and in others not presented) we find this not to be the case: β measured on the embedded space would predict too large a mean energy if applied to the logical problem.

Since the objective may be to sample at larger inverse temperature in the logical space, we must consider whether inclusion of the chain-broken samples (whether by chain-voting, or some other mechanism) is valuable. If we restrict to the chain-intact system it seems we have a Boltzmann distribution at significantly lower temperature; including chain-broken states we have more samples, but we also move to smaller β where it is easier to sample by alternative means. Note that the situation in sampling is much more complicated than the situation in optimization - in optimization we do not have to worry about the distribution over the lowest energy states, merely which case is extremal. In this sense projecting samples (e.g., by chain voting) does no harm, whereas this is not true in sampling.

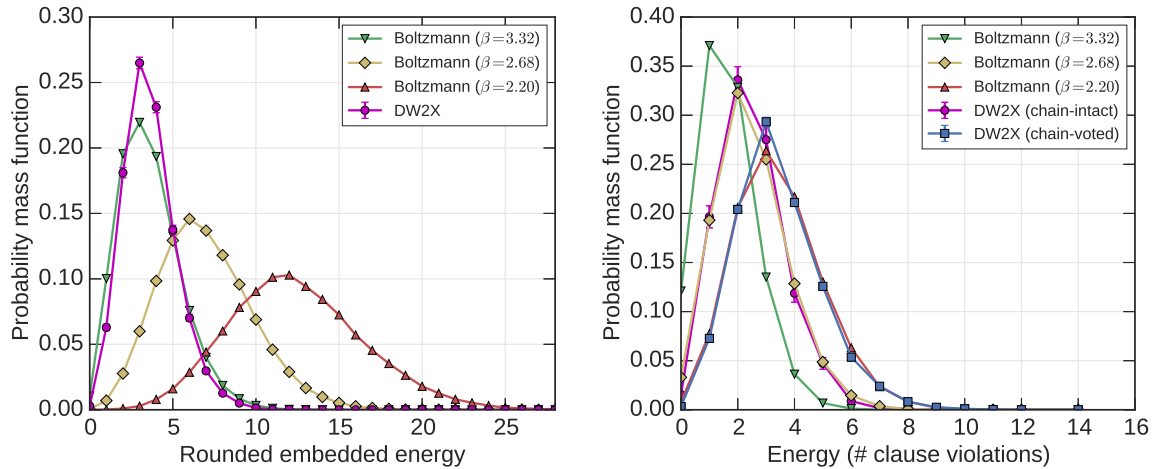


Figure 19: The Boltzmann distribution for the embedded problem (left) differs from the Boltzmann distribution in the logical space (right). The characteristic temperature is also a function of the utilization of samples. To obtain a set of samples in the variable space we either take only those chain-intact samples (discarding all other cases), or we take all samples chain-voted (projecting the chain-broken cases onto chain-intact ones). Whether we include chain-broken samples or not affects the temperature we estimate, as does whether we evaluate in the space of the original problem, or the embedded space.